ISSN 2738-0971
eISSN 2738-1013

Bulletin of Natural Sciences Research

Vol. 12, N° 2, 2022.

BULLETIN OF NATURAL SCIENCES RESEARCH

Published by
Faculty of Sciences and Mathematics, University of Priština in Kosovska Mitrovica
Republic of Serbia

Focus and Scope

Bulletin of Natural Sciences Research is an international, peer-reviewed, open access journal, published semiannually, both online and in print, by the Faculty of Sciences and Mathematics, University of Priština in Kosovska Mitrovica, Republic of Serbia. The Journal publishes articles on all aspects of research in biology, chemistry, geography, geoscience, astronomy, mathematics, computer science, mechanics and physics.

Editorial Office

Ive Lole Ribara 29; 38220, Kosovska Mitrovica, Serbia, e-mail: editor@bulletinnsr.com, office@bulletinnsr.com; fax: +381 28 425 397

Printed by

Sigraf, Ćrila i Metodija bb, 37000 Kruševac, tel: +38137427704, e-mail: stamparijasigraf@gmail.com

Available Online

This journal is available online. Please visit http://www.bulletinnsr.com to search and download published articles.

BULLETIN OF NATURAL SCIENCES RESEARCH

Vol. 12, N^{o} 2, 2022.

CONTENTS

BIOLOGY

CHEMISTRY

GEOGRAPHY, GEOSCIENCE AND ASTRONOMY

MATHEMATICS, COMPUTER SCIENCE AND MECHANICS

Bulletin of Natural Sciences Research
Vol. 12, No. 2, 2022, pp. 1-6.
DOI: https://doi.org/10.5937/bnsr12-35454
Original Scientific Paper

EXTRACT OF *Morinda lucida* LEAF RESCUES HYPOGLYCAEMIC AND DYSLIPIDAEMIC CONDITIONS IN *Plasmodium berghei*-INFECTED MICE

ADAM OLAITAN ABDULKAREEM[1,4,*], ABDULKAREEM OLAREWAJU BABAMALE[2,5], ABASS TOBA ANIFOWOSHE[6,7], OLUFUNKE ADENIKE OPEYEMI[2], NUSIRAT OLORIEGBE[1], COMFORT ADAMOLEKUN[2], SAMSON ADETULA[1], ADEOLA ADEFOLUKE ALA[3]

[1]Animal Physiology Unit, Department of Zoology, University of Ilorin, Ilorin, Nigeria
[2]Parasitology Unit, Department of Zoology, University of Ilorin, Ilorin, Nigeria
[3]Animal Physiology Unit, Department of Zoology, University of Ibadan, Ibadan, Nigeria
[4]Pharmacology Division, CSIR-Central Drug Research Institute, Lucknow, India
[5]Taiwan International Graduate Program in Molecular Medicine, National Yang-Ming Chiao Tung University and Academia Sinica, Taipei Taiwan
[6]Department of Molecular Reproduction, Development and Genetics, Indian Institute of Science, Bangalore, India
[7]Department of Zoology, Faculty of Life Sciences, University of Ilorin, Ilorin, Nigeria

ABSTRACT

Increasing drug resistance is a great threat to malaria control. Therefore, a continuous investigation into alternative therapy to mitigate malaria-associated damages is important. In this study, we investigated the anti-hypoglycaemic and anti-hyperlipidaemic effects of aqueous extract of *Morinda lucida* leaf in *Plasmodium berghei*-infected mice. Twenty-five mice were randomly grouped into five: Uninfected, infected-untreated, chloroquine (20 mg/kg, per oral), and extract-treated (400 mg/kg and 800 mg/kg, respectively, per oral) groups. Fasting blood glucose was measured before parasite inoculation and after the last treatment. Blood was collected for lipid profile assay at the end of the 4-day treatment. Our results revealed that both chloroquine and the extract lowered parasite growth ($p < 0.05$), while chloroquine and 400 mg/kg of the extract improved blood glucose in *Plasmodium berghei*-infection. More so, all the treated groups showed attenuated *Plasmodium berghei*-induced dyslipidaemia, with 400 mg/kg of the extract exhibiting better efficacy. Therefore, this study suggests that *Morinda lucida* leaf extract can be harnessed as a therapeutic regimen for improved malaria treatments and associated complications. Further study is recommended to elucidate the mechanism of anti-hypoglycaemic and anti-hyperlipidaemic activities of the extract and the possible bioactive compound(s) involved.

Keywords: Malaria, Hypoglycaemia, Dyslipidaemia, *Morinda lucida*, *Plasmodium berghei*.

INTRODUCTION

Despite a remarkable reduction in global incidence and mortality rate in the previous decade, malaria remains one of the life-threatening diseases, especially in sub-Saharan Africa and Southeast Asia (WHO, 2020). As of 2018, these regions accounted for approximately 85% of global malaria deaths, most of which occur in children under five. Meanwhile, Nigeria with 23%, leads the six most affected countries, followed by the Democratic Republic of the Congo (11%). Others include the United Republic of Tanzania (5%), Burkina Faso, Mozambique, and Niger (4% each) (WHO, 2019). The majority of malaria-related death in sub-Saharan Africa, including Nigeria, is attributed to *Plasmodium falciparum* (Satish & Ranjana, 2013; Oladeji et al., 2020a) with complex pathological progression as previously reported (Babamale et al., 2017; Geleta & Ketema, 2016; Plewes et al., 2018).

During adaptation to the intracellular compartment of the host's erythrocyte, *Plasmodium* spp. require a large amount of glucose. Therefore, they increase their hexose permeability through hexose transporter of the erythrocyte for improved glucose uptake that then results in reduced host blood glucose level -a condition called hypoglycemia, accompanied by suppression of erythropoiesis (Zijlmans et al., 2014; Pathak & Gosh, 2016). This is the hallmark of several pathological conditions such as anaemia, thrombocytopenia, and nutrient deficiency that are associated with severe malaria, as reported (Slavic et al., 2010; Babamale et al., 2017; Plewes et al., 2018).

Lipid derangement is another diagnostic and prognostic indicator of parasitic infection, including malaria (Mohapatra et al. 2014, Kullu et al., 2018). Lipids play crucial roles in *Plasmodium* spp. metabolism, facilitating their proliferation and transmission (Gulati et al., 2015; Kilian et al., 2018). Their quest

*Corresponding author: abdulkareem.ao@unilorin.edu.ng

for host lipids during the pre-erythrocytic stage of development leads to a lipid homeostatic imbalance and hepatocellular damage (Warjri et al., 2016).

Multiple drug resistance has been a major setback in combating malaria and its complicated outcome until the discovery of Artemisinin-based Combination Therapy (ACT) in the 20th century. The efficacy of ACT was again short-lived by resistance (WHO, 2015), thus necessitating the continuous search for alternative antimalarial drugs that are not only safe but are also accessible and affordable. In many African countries, the use of medicinal plants and their products has gained tremendous recognition as an alternative treatment strategy for many infectious diseases, including malaria (Idowu et al., 2010; Oladeji et al., 2020b). One of such medically-important plants is *Morinda lucida*- a tropical rainforest plant (family Rubiaceae) which occurs throughout the year in the South-Western part of Nigeria (Adeneye, 2013; Adeleye et al., 2018; Oladeji et al., 2020a).

Despite the wide usage of crude extracts of the plant for local malaria treatment in Nigeria (Adebayo et al., 2010, Idih et al., 2017; Afolabi & Abejide, 2020), information regarding the efficiency of *M. lucida* on malaria-induced hypoglycaemia and dyslipidaemia is scarce. Therefore, this study investigated the effect of aqueous leaf extract of *M. lucida* on blood glucose and lipid profile in *P. berghei*-infected mice. We reported that the extract has the potential to ameliorate pathological alterations in the glucose and lipid profiles of the infected mice.

MATERIALS AND METHODS

Plant collection, identification and extraction

The fresh leaves of *M. lucida* were obtained from Rot-Tund farms Nigeria investment limited, Ila-Orangun, Osun State, Nigeria, and identified at Forest Research Institute of Nigeria, Ibadan, Nigeria. The modified method of Ojewunmi et al. (2013) was used for the extraction. Briefly, the plant was thoroughly washed, air-dried at room temperature, and macerated. Macerated leaf (100 g) was soaked in 1000 mL of distilled water and stirred intermittently for 24 hours. Thereafter, the mixture was filtered with muslin cloth and then with filter paper. The filtrate was evaporated to dryness using a rotary evaporator at 55^0C. The extract was refrigerated at 4 ^{0}C before use.

Experimental animals

Twenty-five male Swiss albino mice with an average weight of 20g were obtained from the central animal house, Department of Anatomy, University of Ibadan, Ibadan Oyo state. They were subsequently transferred to the animal house, Zoology department, University of Ilorin, for acclimation and experimental set-up under standard conditions including free access to food and clean water. The rats were handled in accordance with the rules and regulations of the Animals Care and Use Committee (ACUC) and the Institutional Ethical Review Board of the University of Ilorin throughout the study.

Parasite inoculation

Plasmodium berghei (ANKA strain)-bearing mice were obtained from the laboratory, Biochemistry Department, University of Ilorin, Ilorin, Nigeria. 1ml of blood was taken from donor mice and diluted with normal saline; such that 0.2 ml of the infected blood contained inoculums of 1×10^7 infected red blood cells. Twenty out of the total used parasite-free mice were inoculated intraperitoneally with 0.2 ml of infected blood and parasites were allowed to incubate before treatment commenced.

Experimental design and animal grouping

After parasite incubation, the mice were randomly grouped as follows: Groups 1 (uninfected) and 2 (infected-untreated): received distilled water. Group 3 (chloroquine): infected and treated with 20 mg/kg body weight (b.w) chloroquine. Groups 4 and 5 (extract): infected and treated with 400 mg/kg and 800 mg/kg b.w aqueous extract of *M. lucida* leaf, respectively. Both the vehicle (distilled water) and the extract were orally administered for 4 days.

Estimation of parasitaemia and percentage parasite inhibition

Blood was obtained from the caudal tip of the animals on the first treatment day (Day 0), smeared on a clean glass slide, and stained with Giemsa for parasite count. The procedure was repeated on Days 2 and 4. The parasitaemia and percentage (%) parasite inhibition were then determined as previously described (Adetutu et al., 2016).

Blood glucose determination

The blood glucose was measured by obtaining a drop of blood from the tail after a 24hr fast using a Glucometer (Elased et al., 1996). Fasting blood glucose was measured before parasite inoculation and after the last treatment.

Lipid profile assay

Estimations of total cholesterol (TC) and triglyceride (TG) were carried out by colorimetric methods, using assay kit obtained from Fortress Diagnostics Ltd. (Antrim, United Kingdom). High-density lipoprotein (HDL)-cholesterol concentration was estimated using the precipitation method of Warmick et al. (1982), while low-density lipoprotein (LDL)-cholesterol was estimated using modified Friedewald's formula (Friedewald et al., 1972).

RESULTS

Aqueous extract of Morinda lucida inhibits plasmodia growth in P. berghei mice

The efficacy of malaria therapy is a measurement of its ability to reduce the burden of the infection associated with

parasite proliferation. Our data in Table 1 show that *P. berghei* infection significantly increased (p <0.05) parasitaemia after a 4-day curative test. However, treatments with chloroquine (CQ) and aqueous leaf extract of *M. lucida* lowered (p <0.05) the parasitaemia and significantly inhibited (p <0.05) parasite proliferation (Fig. 1). Percentage parasite inhibition recorded in the CQ-treated group (75.88 %) was higher than the values observed in groups treated with 400 mg/kg extract (52.79 %) and 800 mg/kg extract (51.34 %).

Table 1. Effect of aqueous extract of *Morinda lucida* on parasitaemia (% infected RBC) in *Plasmodium berghei*-infected mice. Both chloroquine and aqueous extract of *M. lucida* leaf significantly lowered parasitaemia in *P. berghei*-infected mice.

Parasitaemia(%)			
GROUPS	**DAY 0**	**DAY 2**	**DAY 2**
Uninfected	0.00 ± 0.00	0.00 ± 0.00	0.00 ± 0.00
Infected untreated	27.32 ± 0.61	36.40 ± 3.58	41.22 ± 3.49*
CQ	89.95 ± 5.45	27.15 ± 1.73***	21.70 ± 2.30***
400mg/kg	64.60 ± 2.31	56.60 ± 6.57	30.50 ± 1.73**
800mg/kg	39.25 ± 6.00	34.00 ± 2.31	19.10 ± 1.15*

$^{*}p$ < 0.05 vs Day 0; $^{**}p$ < 0.01 vs Day 0; $^{***}p$ < 0.001 vs Day 0 (n=3).

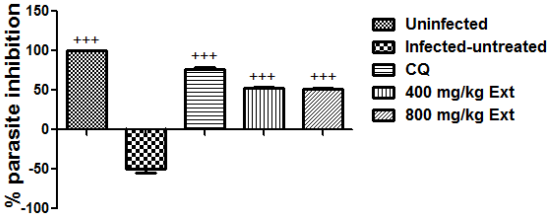

Figure 1. Inhibitory effect of chloroquine (CQ) and aqueous extract of *Morinda lucida* (Ext) on *P. berghei* growth in mice. There was progressive parasite growth in the infected-untreated group, whereas, CQ and Ext significantly inhibited parasite growth, on Day 4 post-treatment. Values were expressed as mean ± S.E.M of 3 mice per group (+++ p < 0.001 vs infected-untreated).

Aqueous extract of Morinda lucida improves fasting blood glucose and lipid profile

Hypoglycaemia and lipid derangements are important prognostic indicators of malaria complications; hence, amelioration of hypoglycaemia and dyslipidaemia offers a better treatment option in malarial infection. Our results reveal that, *Plasmodium berghei* infection significantly lowered fasting blood glucose level by Day 4 post-treatment (p <0.05) compared with the uninfected group (Fig 2). In contrast, both chloroquine and 400 mg/kg *M. lucida* aqueous leaf extract improved the fasting blood glucose. On the other hand, total cholesterol (TC) and low-density lipoprotein-cholesterol (LDL-c) levels were higher (p <0.05) in the infected-untreated group compared with the uninfected group (Table 2). Treatments with chloroquine and aqueous leaf extract of *M. lucida* significantly reduced (p <0.05) both TC and LDL-c, with the best effect in 400 mg/kg extract. No significant differences were observed in triglycerides and high-density lipoprotein-cholesterol (HDL-c) levels, though; there was a slight decrease in HLD-c level in the infected-untreated level when compared with the uninfected group which was relatively improved in all the treated groups.

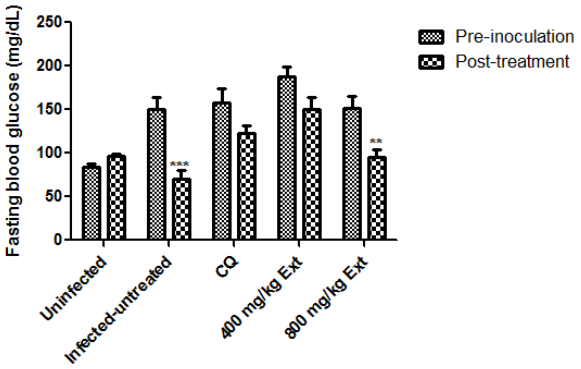

Figure 2. Effect of chloroquine (CQ) and aqueous extract of *Morinda lucida* (Ext) on fasting blood glucose in *Plasmodium berghei*-infected mice. *P. berghei* infection significantly decreased (p <0.001) fasting blood glucose in mice while both CQ and 400 mg/kg Ext improved the fasting blood glucose after 4-day treatment. Values were expressed as mean ± S.E.M of 3 mice per group (** p <0.01 vs pre-inoculation of the same group; *** p <0.001 vs pre-inoculation of the same group).

Table 2. Effect of aqueous extract of *Morinda lucida* on lipid profile (mg/dL) in *Plasmodium berghei*-infected mice. Both chloroquine and aqueous extract of *M. lucida* significantly reduced total cholesterol and low-density lipoprotein cholesterol in *P. berghei*-infected mice.

Parameters (mg/dL)	**Uninfected**	**Infected-untreated**	**CQ**	**400 mg/kg Ext**	**800 mg/kg Ext**
Total Cholesterol	104.4 ± 8.08	143.4 ± 5.19*	100.2 ± 6.35^{++}	90.75 ± 5.19^{++}	113.7 ± 5.75
Triglyceride	62.90 ± 2.88	62.73 ± 1.73	72.93 ± 4.04	63.57 ± 2.88	50.72 ± 4.61
HDL-c	54.13 ± 2.88	46.69 ± 2.88	47.11 ± 4.04	50.41 ± 2.30	49.59 ± 2.88
LDL-c	64.92 ± 4.04	109.2 ± 8.08**	67.72 ± 5.19^{++}	53.25 ± 5.77^{+++}	74.25 ± 6.92^{+}

$^{*}p$ < 0.05 vs uninfected; $^{**}p$ < 0.01 vs uninfected; +p <0.05 vs infected-untreated; ++p <0.01 vs infected-untreated ^{+++}p < 0.001 vs infected-untreated (n=3). HDL-c, high-density lipoprotein-cholesterol; LDL-c, low density lipoprotein-cholesterol.

DISCUSSION

The pathological impact of aqueous leaf extract of *M. lucida* was investigated in this study. The results showed that 400 mg/kg and 800 mg/kg aqueous extract of *M. lucida* leaf significantly reduced *P. berghei* proliferation in mice. We also showed that the extract (400 mg/kg) improved fasting blood glucose and dyslipidaemia in *P. berghei* infection. Comparatively, our findings emphasized that 400 mg/kg of aqueous leaf extract of *M. lucida* efficiently ameliorated *P. berghei*-associated dyslipidaemia better than 800 mg/kg of the extract and chloroquine.

Our findings of a higher curative effect in rats treated with 400 mg/kg extract, compared to those treated with 800 mg/kg, agree with the previous study of Afolabi and Abejide (2020) where the lowest of the used doses of *M. lucida* plant extract showed a highest curative effect in *P. berghei*-infected mice. However, 52.79 % parasite inhibition observed in the 400 mg/kg extract-treated group of this study is lower than the 83 % curative effect reported in their study. Similarly, the anti-plasmodial activity of *M. lucida* leaf extract reported in our study is lower than that earlier reported by Idowu et al. (2014). The difference in these findings may be due to the different extracting solvents used, period of extraction, and/or varied sites of leaf collection. Extracting solvent and the geographical location of a plant are key important factors that affect the quantitative yield of a plant's bioactive components, thereby affecting its presumed medicinal activity (Sultana et al., 2009; Gupta et al., 2011).

Hypoglycaemia is a common complication of malaria in pregnant women and children, which increases the risk of mortality in them (Ounjaijean et al., 2019). In this study, *P. berghei* infection resulted in decreased fasting blood glucose. This concurs with previous findings (Sihabud et al., 2015; Ounjaijeana et al., 2018). Although the underlying mechanism of hypoglycaemia in malaria is not well understood, increasing evidence suggests that suppression of gluconeogenesis by the parasites, and the host's inability to compensate for the parasite glucose uptake play major roles (Mehta et al., 2005; Zijlmans et al., 2014). Thus, the hypoglycaemia observed in this study following *P. berghei* infection may be attributed to increased glucose uptake by the parasite without compensatory production in the hosts. Administration of 400 mg/kg aqueous extract of *M. lucida* leaf improved blood glucose level, which compares favourably with chloroquine's effect. The observed improvement in blood glucose in the 400 mg/kg administered group may imply that the lower dose of *M. lucida* leaf extract enhanced gluconeogenesis in the hosts or it inhibited hexose transporter of the infected erythrocytes, thereby decreasing glucose uptake by the parasite (Ruan et al., 2012; Ahmad et al., 2016). Lipid metabolism is compromised during the exoerythrocytic stage of *Plasmodium* in parenchyma and Kupffer cells, leading to alterations in lipid profile and subsequently dyslipidaemia (Oluba et al., 2012). The present study shows evidence of dyslipidaemia in *P. berghei* infection. This is in conformity with the previous studies that demonstrated increased TC and LDL-c in human and rodent malaria (Ngou-Milama et al., 1995; Krishna et al., 2009; Jacob, 2014) and rodents (Joshua et al., 2020). Treatments with both chloroquine and the extract lowered TC and LDL-c in *P. berghei*-infected mice, suggesting the efficiency of the extract in mitigating malaria-induced dyslipidaemia. However, a better ameliorative effect was observed in the 400 mg/kg extract-treated group. This may imply that aqueous extract of *M. lucida* leaf at 400 mg/kg possesses a better therapeutic potential to suppress dyslipidaemia in malaria than chloroquine.

Aqueous leaf extract of *M. lucida* has been previously shown to possess flavonoids, among other bioactive components (Unekwuojo et al., 2011). Flavonoids are known for their antioxidant and anti-inflammatory properties. They can also inhibit low-density lipoprotein (LDL) oxidation and regulate serum lipid metabolism (Kerry & Abbey, 1997; Chen et al., 2011). Therefore, the anti-hyperlipidaemic effect of *M. lucida* leaf extract observed in the present study may be due to the bioactive components of the extract, especially flavonoids, which then aid in bringing lipid metabolism back to normal.

CONCLUSION

This study justifies the common practice of using *M. lucida* crude extracts for malaria treatment in the South-Western part of Nigeria. It also demonstrates that the aqueous extract of *M. lucida* leaf improved blood glucose and ameliorated lipid profile derangement in *P. berghei*-infected mice. We, therefore, suggest that *M. lucida* leaf extract can be harnessed as a therapeutic regimen for better treatment of malaria and associated complications. Further study is recommended to investigate the mechanism of anti-hypoglycaemic and anti-hyperlipidaemic activities of the extract and the possible bioactive compound(s) involved.

REFERENCES

Adebayo, N. S., Abubakar, A. A., Emmanuel, A. S., Oluwabunmi, S. B., Ifeoluwa, J. D. & Blessing, O. 2020. Phyto Chemical Screening and Antiplasmodial Potential of Morinda lucida (Brimstone Leave) In Infected Mice. J. Middle East North Afr. sci.

Adeleye, O. O., Ayeni, O. J. & Ajamu, M. A. 2018. Traditional and medicinal uses of *Morinda lucida*. J. Med. Plants.

Adeneye, A. A. 2013. Profile of *Morinda lucida* leaf fractions on blood glucose and lipids in normal and Alloxan-induced hyperglycaemic rats. *Pharmacologia*.

Adetutu, A., Olorunnisola, O. S., Owoade, A. O., Owoade, A O. & Adegbola P. 2016. Inhibition of in vivo growth of *Plasmodium berghei* by *Launaeataraxacifolia* and

Amaranthus viridis in mice. Malar Res Treat. https://doi.org/10.1155/2016/9248024

Afolabi, O. J. & Abejide, A. E. 2020. Antiplasmodial activities of Morinda lucida (Benth) and *Alstoniaboonei* (De wild) in mice infected with *Plasmodium berghei*. Bulletin of the National Research Centre. https://doi.org/10.1186/s42269-020-00342-8

Ahmad, W., Jantan, I. & Bukhari, S. N. 2016. *Tinosporacrispa* (L.) Hook. f. & Thomson: A Review of Its Ethnobotanical, Phytochemical, and Pharmacological Aspects. Front. Pharmacol**.** https://doi.org/10.3389/fphar.2016.00059

Babamale, O. A., Abdulkareem, A. O., Akande, A. O., Afolayan, M. A. & Ugbomoiko, U. S. 2017. Malaria-induced anaemia and serum micronutrients in asymptomatic Plasmodium falciparum infected patients. J Parasit Dis.

Babamale, O. A., Abdulkareem, A. O., Opeyemi, O. A. & Ugbomoiko, U. S. 2017. Alterations in T-helper cell type 1 and blood cell parameters in malaria-infected patients. Egypt. j. basic appl. sci. http://doi10.1007/s12639-017-0940-4

Chen, L., Ma, X. B., Liang, Y. H., Pei, S. C., Feng, Y. P. & Wei, M. 2011. Effects of persimmon leaf total flavonoid on enzyme of lipoprotein metabolism and antioxidation in hyperlipidemia rats. Chin. J. Nat. Med.

Elased, K. M., Taverne, J. & Playfair, J. H. L. 1996. Malaria, blood glucose, and the role of tumour necrosis factor (TNF) in mice. Clin Exp Immunol. 105, pp. 443-449.

Friedewald, W. T, Levy, R. I. & Fredrickson, D. S. 1972. Estimationof the concentration of lowdensity lipoprotein cholesterol in plasma, without use of the preparativeultracentrifuge. Clin Chem.

Geleta, G. & Ketema, T. 2016. Severe Malaria Associated with Plasmodium falciparum and P. vivax among Children in Pawe Hospital, Northwest Ethiopia. Malar Res Treat. http://dx.doi.org/10.1155/2016/1240962

Gulati, S., Ekland, E. H., Ruggles, K. V., Chan, R. B., Jayabalasingham, B., Zhou, B., Mantel P. Y., Lee M.C., Spottiswoode, N., Coburn-Flynn O., Hjelmqvist D., Worgall T. S., Marti M., Di Paolo G. & Fidock D. A. 2015. Profiling the essential nature of lipid metabolism in asexual blood and gametocyte stages of Plasmodium falciparum. Cell Host Microbe**.**

Gupta**,** S**.**, Bhaskar**,** G**.** & Andola C. H. 2011. Altitudinal variation in essential oil content in leaves of Zanthoxylum alatum a high value aromatic tree from Uttarakhand. Res. J. Med. Plants.

Idih, F. M., Ighorodje-Monago, C. C. & Ezim O. E. 2017. Antiplasmodial Effect of Ethanol Extract of Morinda lucida and Mucuna pruriens Leaves on NK65 Chloroquine Resistant Strain of *Plasmodium berghei* in Mice. Clin Exp Pharmacol. https://doi.org/10.4172/2161-1459.1000234

Idowu**,** O. A., Babalola**,** A. S., Adenubi**,** O. T. & Olukunle**,** J. O. 2014. Anti-plasmodial activities of combined extracts of *Morinda morindiodes*, *Morinda lucida* and *Vernonia amygdalina* in *Plasmodium berghei* infected-mice. Zoologist (The).

Idowu, O. A., Soniran, O. T., Ajana, O. & Aworinde, D. O. 2010. Ethnobotanical survey of antimalarial plants used in Ogun State, Southwest Nigeria. Afr. J. Pharm. Pharmacol.Jacob**,** E. A. 2014. Assessment of Altered Plasma Lipid Pattern in *Plasmodium Falciparum* Malaria Infected and Non Infected Individuals. Int J Blood Res Disord.

Jacob E. A. 2014. Assessment of Altered Plasma Lipid Pattern in *Plasmodium Falciparum* Malaria Infected and Non Infected Individuals. Int J Blood Res Disord. https/doi.org/10.12691/ijhd-1-1-5

Joshua, P. E., Okoro, I. J., Ekpo, D. E., Okagu, I. U. & Ogugua V. N. 2020. Methanol extract of Erythrina senegalensis leaves (MEES) ameliorates Plasmodium berghei-ANKA 65-parasitised aberrations in mice. All Life. https//doi.org/10.1080/26895293.2020.1718777

Kerry, N. & Abbey M. 1997. Red wine and fractionated phenolic compounds prepared from red wine inhibit low density lipoprotein oxidation in vitro. Atherosclerosis.

Kilian, N., Choi, J., Voelker, D. R. & Mamoun, C. B. 2018. Role of phospholipid synthesis in the development and differentiation of malaria parasites in the blood. J. Biol. Chem.

Krishna, A. P., Chandrika, Kumar S., Acharya, M. & Patil S. L. 2009. Variation in common lipid parameters in malaria infected patients. Indian J PhysiolPharmacol**.**

Kullu, B. K., Majhi, C., Pradhan, B. & Swain, D. K. 2018. Lipid profiles among Plasmodium falciparum infected, non malarial febrile patients and volunteers. Int J Adv Med.

Mehta, M., Sonawat, H. M. & Sharma, S. 2005. Malaria parasite-infected erythrocytes inhibit glucose utilization in uninfected red cells. FEBS Lett.

Mohapatra, S., Samantaray, J. C. & Ramakrishan, L. 2014. Lipid derangement as diagnostic and prognostic indicator for visceral leishmaniasis. Trop Parasitol.

Ngou-Milama, E., Duong, T. H., Minko, F., Dufillot, D., Kombila, M., Richard-Lenoble, D. & Mouray, H. 1995. Lipid profile during specific malaria therapy in Gabonese children (in French). Sante.

Ojewunmi, O., Oshodi T., Ogundele, O., Micah, C. & Adenekan S. 2013. Evaluation of the Anti-Diabetic and Antioxidant Activities of Aqueous Extracts of *Morinda lucida* and *Saccharum officinarum* Leaves in Alloxan-Induced Diabetic Rats. Int J Biochem Res Rev**.**

Oladeji, O. S., Odelade, K. A. & Oloke J. K. 2019. Phytochemical screening and antimicrobial investigation of *Moringa oleifera* leaf extracts. J. Sci. Technol. Innov. Dev.

Oladeji, O. S., Oluyori, A. P., Bankole, D. T. & Afolabi, T. Y. 2020. Natural Products as Sources of Antimalarial Drugs: Ethnobotanical and Ethnopharmacological Studies. Scientifica. https://doi.org/10.1155/2020/7076139

Oluba, O. M., Olusola, A. O., Eidangbe, G. O., Babatola, L. J. & Onyeneke E. C. 2012 Modulation of lipoprotein cholesterol levels in Plasmodium berghei malarial infection by crude aqueous extract of Ganoderma lucidum. Cholesterol.

Ounjaijeana**,** S., Chachiyob**,** S. & Somsak V. 2019. Hypoglycemia induced by Plasmodium berghei infection is prevented by treatment with *Tinosporacrispa* stem extract. Parasitol. Int.

Pathak V. A. & Ghosh K. 2016. Erythropoiesis in Malaria Infections and Factors Modifying the Erythropoietic Response. Anemia. https://doi.org/10.1155/2016/9310905

Plewes, K., Turner, G. D. H. & Dondorp, A. M. 2018. Pathophysiology, clinical presentation, and treatment of coma and acute kidney injury complicating falciparum malaria. CurrOpin Infect Dis.

Ruan, C. T., Lam, S. H., Chi, T. C., Lee, S. S. & Su, M. J. 2012. Borapetoside C from *Tinosporacrispa* improves insulin sensitivity in diabetic mice. Phytomedicine.

Satish, B. & Ranjana, K. 2013. Herbal plants used for the treatment of malaria- a literature review. J PharmacogPhytochem.

Sihabud, M., Yongthawee, P., Chutoam, P., Klongthalay, S. & Somsak V. 2015. Effect of Black Tea Extract on Hypoglycemia Induced by *Plasmodium berghei* ANKA Infection in Mice. Malar Cont Elimination.

Slavic, K., Straschil, U., Reininger, L., Doerig, C., Morin, C., Tewari, R. & Krishna, S. 2010. Life cycle studies of the hexose transporter of Plasmodium species and genetic validation of their essentiality. Mol. Microbiol.

Sultana, B., Anwar, F. & Ashraf M. 2009. Effect of Extraction Solvent/Technique on the Antioxidant Activity of Selected Medicinal Plant Extracts. Molecules. https//doi.org/10.3390/molecules14062167

Unekwuojo, E. G., James, O. & Olubunmi A. R. 2011. Suppressive, Curative and Prophylactic Potentials of Morinda lucida (Benth) against Erythrocytic Stage of Mice Infective Chloroquine Sensitive *Plasmodium berghei* NK-65. Br J Appl Sci Technol.

Warjri, S. B., Ete, T., Mishra, A., Barman, B., Mishra, J., Pala, S., Beyong, T. & Issar, N. K. 2016. Association between Clinical Malaria and Blood Lipids in North Eastern India.

Warmick, G. R., Benderson, J. & Albers, J. J. 1982. Dextran sulphate-Mg^{2+} precipitation procedure for quantitation of high-density lipoprotein cholesterol. Clin Chem.

WHO, World Malaria Report 2015. World Health Organization, Geneva, Switzerland.

WHO, World Malaria Report 2019. World Health Organization, Geneva, Switzerland.

WHO, World Malaria Report 2020. World Health Organization, Geneva, Switzerland.

Zijlmans, W. C., van Kempen, A. A., Serlie, M. J., Kager, P. A. & Sauerwein, H. P. 2014. Adaptation of glucose metabolism to fasting in young children with infectious diseases: a perspective. J Pediatr Endocrinol Metab.

Bulletin of Natural Sciences Research
Vol. 12, No. 2, 2022, pp. 7-13.
DOI: https://doi.org/10.5937/bnsr12-39835
Original Scientific Paper

QUALITY EVALUATION OF WINES FROM KOSOVO AND METOHIJA: POLYPHENOLS CONTENT, ANTIOXIDANT ACTIVITY AND ELEMENTAL COMPOSITION

SONJA JEVTIĆ[1], JELENA MUTIĆ[2], SLADJANA DJURDJIĆ[2], LJILJANA BABINCEV[3], DEJAN GUREŠIĆ[4], DALIBOR M. STANKOVIĆ[2], BRANKA B. PETKOVIĆ[4*]

[1]Hign School „Nikola Tesla“, Leposavić, Serbia
[2]Faculty of Chemistry, University of Belgrade, Belgrade, Serbia
[3]Faculty of Technical Sciences, University of Priština in Kosovska Mitrovica, Kosovska Mitrovica, Serbia
[4]Faculty of Sciences and Mathematics, University of Priština in Kosovska Mitrovica, Kosovska Mitrovica, Serbia

ABSTRACT

Wine is a very rich source of polyphenols and essential elements which have multiple biological activities. This study evaluates the total phenolic content (TPC), antioxidant activity (AA) of sixteen wine samples made from different grape varieties in the territory of Kosovo and Metohija, mostly from the area of Orahovac and Velika Hoča. The obtained results, determined by using the Folin-Ciocalteu assay, showed that wines from territory of Kosovo and Metohija are rich in polyphenols, with TPC ranges from 276±16 to 371±46 (white wines) and 1467±32 to 2823±43 mg gallic acid equivalents GAE/L (red wines). The total antioxidant activities, determined by ABTS method, range from 8.7±0.4 to 22.8±0.7 mmol trolox equivalents TE/L for red wines and from 1.3±0.1 to 3.8±0.3 mmol TE/L for white wines. Elemental content of studied wines showed certain difference between wines from nearby regions.

Keywords: Polyphenols, Antioxidant activity, Wine, Elemental composition.

INTRODUCTION

Viticulture and enology are very long-standing in Kosovo and Metohija. This region is located in the central part of the Balkan Peninsula, in southeastern Europe with an average altitude of about 800 m, but with a pronounced height change of the relief and morphology. The importance of wine cultivation and wine production in the territory of Kosovo and Metohija is not at random because the aforementioned territory, especially Metohija, has exceptional climatic and geographical conditions for its cultivation (Ivanišević & Jakšić, 2012). Climatic conditions and soil type are favorable for autochthonous grape varieties which are specific for this part of Balkan Peninsula (Prokupac, Vranac, Smederevka, Župljanka, Kraljica, Žilavka), while other European grape varieties like Gamay, Italian riesling, Cabernet sauvignon, Merlot, are also adopted to this area.

Phenolic compounds have long been considered to be basic components of wines and over 200 compounds have been identified. Wine composition, including the contents of phenolic compounds, varies markedly depending on the grape cultivar, soil, nutrition, climatic conditions, weather, winemaking procedure, and conditions of maturation and storage (Stratil et al., 2008). Different grape varieties also show a distinct sensory appeal, chemical composition, different quantities of native antioxidants and therefore different biological activity (Menković et al., 2014). The anti-oxidant activity of wines has been related to their polyphenolic constituents and is mainly based on their free radical scavenging capacity (Sánchez-Moreno et al., 1999). The total phenols in wines are mainly determined by spectrophotometric Folin-Ciocalteu assay (Waterhouse, 2016.) while HPLC is widely used for individual identification and quantification of polyphenols (Rastija & Medić-Šarić, 2009; Šeruga, 2011). Various methods for determination of antioxidant activity could be used (mostly spectrometry, then electrochemical techniques and chromatography) (Pisoschi & Negulescu, 2011; Stratil, 2008).

It is well known that metals effect on sensorial characteristics, flavor and aroma of wine. Chemical composition of wine provides viticulturists to control the process of vinification in order to obtain high quality wine. The presence of some metals in wines such as Al, Zn, Cu, Fe, Pb is important for efficient alcoholic fermentation (Stafilov & Karadjova, 2006). When considering winemaking and quality assurance of branded wines, knowledge of metal is of special economic importance (Pohl, 2007) Evaluation of amounts of major and trace elements is important for establishment of elemental profiles of studied wines.

According to literature, there is only study of Metohian wines in terms of spectrophotometric color characterization (Babincev et al., 2016), but there is no report about wine quality, considering polyphenols content, antioxidant activity

*Corresponding author: branka.petkovic@pr.ac.rs

and chemical composition of wines from territory of Kosovo and Metohija. Comparison of this results and literature data for wines from neighboring regions and countries, bearing in mind varieties of grapes from which the wines were made, could offer interesting and important facts.

EXPERIMENTAL

Chemicals and apparatus

Gallic acid (3,4,5-trihydroxybenzoic acid), Folin-Ciocalteu reagent, trolox (6-hydroxy-2,5,7,8-tetramethylchroman-2-carboxylic acid) and ABTS (2,2'-azinobis-(3-ethylbenzothiazoline)-6-sulfonic acid) were products of Sigma Aldrich, Germany. All the other chemicals were analytical grade.

Spectrophotometric measurements of colour, TP and AA determination of wine samples were done on Rayleigh VIS-7220G/UV-9200 Spectrophotometer (Beijing Beifen-Ruili Analytical Instrument Group Co. Ltd.

Inductively Coupled Atomic Emission Spectrometer, ICP-OES (iCAP 6500 Duo Thermo Scientific, UK) and inductively coupled plasma mass spectrometer (ICP-Q-MS, Thermo Scientific Xseries 2, UK) were used for determination of major and trace elements, respectively. ICP multi-element stock solutions (VHG standards, Manchester, UK) containing 1000 mg/L were used as stock solution for calibration. Mix of ^{6}Li, ^{45}Sc, ^{115}In and ^{159}Tb (VHG standards, Manchester, UK) were used as internal standards for ICP MS measurements.

Wine samples

The basic data about wine samples (vintages 2012, 2013 and 2015) are presented in Table 1. Most of samples are from Velika Hoča and Orahovac. Four white wines are analyzed (samples 2, 4, 5, and 16), one is rose (12) and the others are red. Two wines are commercially available: sample No 12, Duša Metohije, from private winery of Lj. Đurišić and sample No 13, Manastirsko Dečansko. Other wines are produced in domestic production or small private (or monastery) wineries. All wines are stored in the refrigerator to +4 °C, and filtered through syringe filter before determination. pH of wine samples ranged from 3.19-3.84.

For determination of elements content in wine, samples were diluted (1:10) with water containing 2 % (v/v) of nitric acid (Merck, Germany). Standards were prepared with 1% (v/v) ethanol and 2% (v/v) nitric acid and in order to provide the same matrix as in samples.

Determination of total phenolic content

The total phenolic content of wines was determined by using the Folin-Ciocalteu assay. The standard solutions of gallic acid (50, 100, 150, 250 and 500 mg/L) were prepared. Folin-Ciocalteu's phenol reagent and 25% Na_2CO_3 solution were added according the procedure (Waterhouse, 2016.) to each standard solution and to the reagent blank. After incubation for 90 min at room temperature in the darkness, the absorbance against prepared reagent blank was determined at 750 nm. Total phenolic content of wines was expressed as mg of gallic acid equivalents GAE/L. 20μL of sample was added for red wines determination, and 200μL for white wines. All samples were analyzed in triplicates.

Table 1. Basic facts about wine samples.

Sample	Wine colbr	Grape variety	Area, winery
1	Red	Vranac	Velika Hoča
2	White	Smederevka	Velika Hoča
3	Red	Prokupac, Vranac	Velika Hoča
4	White	Župljanka	Velika Hoča
5	White	Italian riesling	Orahovac
6	Red	Prokupac, Vranac, Gamay	Orahovac
7	Red	Cabernet sauvignon	Velika Hoča
8	Red	Vranac	Velika Hoča Hočawine d.o.o.
9	Red	Gamay	Velika Hoča Hočawine d.o.o.
10	Red	Merlot	Velika Hoča
11	Red	Tamjanika / (Muscat)	Kosovska Kamenica
12	Red	Vranac, Cabernet sauvignon, Gamay, fruit aromas	Velika Hoča Hočawine d.o.o.
13	Red	Cabernet sauvignon, Merlot, Gamay, Vranac	Orahovac Monastery winery
14	Red	Prokupac	Orahovac
15	Red	Vranac	Gračanica Monastery winery
16	White	Kraljica, Žilavka, Tamjanika/ (Muskat)	Gračanica Monastery winery

Determination of antioxidant activity

ABTS test was performed according to the literature (Cavuldak et al., 2013). ABTS radical is obtained by incubating an aqueous solution of 7 mmol/L ABTS with 2.45 mmol/L $K_2S_2O_8$ for 12-16 hours in the dark, at room temperature. $ABTS^{\bullet+}$ radical solution was prepared freshly on the day of analysis by diluting the stock solution with phosphate buffer (PBS), to an absorbance of 0.70 ± 0.02 at 734 nm. The sample volume of 0.1 cm^3 (differently diluted depending on the sample) was added to 3.9 cm^3 of the working solution of ABTS radical, the solution was mixed well and allowed to stand for 6 minutes in a dark place, and absorbance was measured. Standard Trolox solutions (5–20 mmol/L) were also evaluated against the radical in order to obtain a calibration curve. Results are expressed as Trolox Equivalent Antioxidant Capacity (TEAC).

Determination of elemental composition

Seventeen elements, including major (Ca, Mg, Na, K, Rb, Fe) and trace (Mn, Cu, Zn, V, Co, Ni, Cd, Ba, Cr, Se and Pb) elements, in a set of 16 wine samples were analysed. The analytical lines used for each element, the limit of detection (LOD) as well as ICP OES instrumental conditions are shown in Table 2. Also, measured isotopes and instrument operating conditions for ICP MS determination are given in Table 2.

Table 2. Instrument operating conditions for ICP-OES and ICP-Q-MS.

ICP- OES	
Nebulizer	Concentric
Spray chamber	Cyclonic
Rf power (W)	1150
Principal argon flow rate (L/min)	12
Auxiliary argon flow rate (L/min)	0.5
Nebulizer argon flow rate (L/min)	0.5
Sample flow rate (mL/min)	1
Selected wavelengths (nm)	Fe (259.9); Na (589.5); Ca (373.6); Mg (279.5); K (766.4); Rb (780.0)
Detection limits (µg/L)	Fe (0.2); Na (0.2); Ca (0.3); Mg (0.2); K (0.4); Rb (0.1)
ICP-Q-MS	
Rf power (W)	1548
Gas flows (L/min)	13.9;1.09;0.8
Acquisition time	3 x 50s
Points per peak	3
Dwell time (ns)	10
Detector mode	Pulse
Measured isotopes	^{51}V, ^{59}Co, ^{60}Ni, ^{63}Cu, ^{66}Zn, ^{111}Cd, ^{137}Ba, ^{208}Pb, ^{52}Cr, ^{55}Mn, ^{78}Se
Detection limits (µg/L)	V (0.02), Co (0.02), Ni (0.3), Cu (0.2), Zn (0.4), Cd (0.05), Ba (0.02), Pb (0.1), Cr (0.3), Mn (0.4), Se (0.2)

RESULTS AND DISCUSION

Determination of elemental composition

Results for total phenol content expressed in gallic acid equivalents and antioxidant activity expressed as TEAC for studied wine samples were presented in Table 3. TPC in red wines varied from 1467±32 to 2823±43 mg/L of GAE, and the highest value was for wine produced from Vranac grape variety in 2012. The reason could be that 2012 year was very successful enology year in this area. Sample No 1 with 2595±22 mg/L of GAE was also made from Vranac grape variety in 2015, while wine No 12, Duša Metohije, had a highest TPC for year 2013, and it was made from Vranac, Cabernet sauvignon, Gamay and fruits. Hence, all the red wines, with the exception of two samples made from varieties Merlot and Cabernet Sauvignon, have a polyphenol content between about 1900 and almost 2900 mg/L GAE. As usual, white wines had a much lower TPC then red ones, and TPC was in the range of (276±16 - 371±46 mg/L GAE). The highest content of TPC for white wines was found for wine made from Župljanka grape variety. Should be noted that the sample number 11, made from Tamjanika (domestic name for Muscat de Frontignan variety), have properties of rose wine, because its colour and phenolics content are between red and white wines. It is interesting that wine from native cultivar Prokupac at Metohija territory showed much higher TPC then it was reported for Prokupac wine from central Serbia and the phenolic content was higher than in wines from Merlot and Cabernet Sauvignon cultivators, contrary to Atanacković et al. (Atanacković et al., 2012). Merlot from Istria region, Croatia (2005/2006), had a TPC of 1260±23 (Šeruga et al., 2011) while for Cabernet Sauvignon (1998) and Merlot (1998) grown in Croatia were fond 2402 and 3087 mg/L GAE, respectively (Katalinić et al., 2004). Croatian wines like Ivan Dolac and Dingač, made from native variety Plavac mali had a TPC greater than 3000 mg/L GAE (Šeruga et al., 2011; Katalinić et al., 2004).

Table 3. Total phenolic content and antioxidant activity of wines from Kosovo and Metohija.

Sample	**TPC mg/L GAE**	**AA, TEAC mmol TE/L**
1	2595±22	19±0.5
2	315±35	2.7±0.4
3	1909±28	12±0.8
4	371±46	3.8±0.3
5	295±18	1.8±0.6
6	2400±37	17.2±0.7
7	1613±25	9.8±0.3
8	2823±43	22.8±0.7
9	1918±19	12.5±0.5
10	1467±32	8.7±0.4
11	808±11	4.2±0.2
12	2203±26	16±0.5
13	2041±32	15.8±0.6
14	1901±34	15±0.2
15	2099±27	15.2±0.4
16	276±16	1.3±0.1

TPC contents of Metohija wines made from Smederevka, and Vranac cultivator were higher than reported in neighboring Macedonia (1382±38.2 and 1515±27.6 mg/L GAE) (Ivanova et al., 2010). Based on these results, it can be concluded that conditions in Metohija are very appropriate for Vranac, Gamey, Prokupac, Župljanka and Smederevka cultivars, and wines from Vranac variety certainly had highest content of polyphenols.

Antioxidant activity (AA) is strongly dependent of the type and structure of poliphenols present in wines. AA for studied red wines ranged from 9.8±0.3 to 22.8±0.7 TEAC and for white wines from 1.3±0.1 to 3.8±0.3 mmol TE/L. The lowest antioxidant activity was found for wine samples 7 and 10, made from Cabernet sauvignon and Merlot grape variety. There was a strong correlation between total phenol content (correlation coefficients was R=0.9727).

Elemental profile of wines

Seventeen elements, including major (Ca, Mg, Na, K, Rb, Fe) and trace (Mn, Cu, Zn, V, Co, Ni, Cd, Ba, Cr, Se and Pb) elements, in a set of 16 wine samples were analysed. The results together with summarized parameters (mean, median, minimum, maximum value and standard deviation) obtained for element content in wine samples presented in Table 4 and 5.

The most abundant element in all analysed wine samples was potassium, with content ranging from 300 mg/L (sample 16, white wine from Gračanica Monastery winery) to 657 mg/L (sample 7, red wine from winery Velika Hoča). The obtained results are in accordance with values reported in the literature (Ražić & Onjia, 2010; Đurđić et al., 2017). The highest concentration of potassium in wines could be explained by the fact that it is an essential element for plants, as well as the application of fertilizers on the basis of this metal (Rodrigues et al., 2011). The content of K in the wine also depends on the grape variety, climatic conditions, soil and fermentation temperature. The elements Mg and Ca showed high mean concentrations 89.1 and 62.7 mg/L, respectively. Values obtained for Mg and Ca are similar with results obtained for Macedonian (Ivanova-Petropulos et al., 2013), other Serbian (Đurđić et al., 2017) and Croatian wines (Vinković Vrček et al., 2011).

In this study, results for Rb ranged from 2.08 to 6.27 mg/L, which are higher compare to results obtained by (Geana et al., 2013) for Romanian red and white wines (0.783 mg/L and 1.050 mg/L, respectively) and for other Serbian wines (0.28 to 4.70 mg/L) (Đurđić et al., 2017). Alkaline earth metals and Rb are less affected by technological factors, so they could be the most relevant elements for geographical origin authentication (Pohl, 2007).

Sodium was present with mean value of 13.29 mg/L. These results are lower than literature data where high concentrations of Na in wines explained by small distance from the sea (Iglesiaset al., 2007) but in agreement with results obtained for Macedonian wine (Ivanova-Petropulos et al., 2013), other Serbian (Đurđić et al., 2017) or German wine (Thiel & Danzer, 1997) report that the different elemental content might provide for differences in the process of vinification, difference occurs due to longer contact skin and seeds of grapes with juice during the production of red wines.

Table 4. Results of major elements composition in wine samples.

mg/L	Fe	K	Mg	Ca	Na	Rb
1	2.9 ± 0.03	452 ± 3	116.4 ± 0.1	79.5 ± 0.6	4.2 ± 0.4	5.2 ± 0.2
2	0.75 ± 0.03	452 ± 2	50.3 ± 0.3	67.5 ±0.5	3.8 ± 0.3	4.1 ± 0.2
3	0.23 ± 0.01	573 ± 4	105.7 ± 0.2	59.5 ± 0.6	5.5 ± 0.4	4.3 ± 0.2
4	0.19 ± 0.03	462 ± 4	72.6 ± 0.3	48.1 ± 0.6	4.1 ± 0.4	3.5 ± 0.2
5	1.86 ± 0.03	451 ± 3	70 ± 0.3	74.8 ± 0.5	6.2 ± 0.4	3.1 ± 0.2
6	3.32 ± 0.02	618 ± 5	89.7 ± 0.2	42.6 ± 0.5	1.5 ± 0.4	2.1 ± 0.2
7	9.00 ± 0.01	657 ± 5	137.3 ± 0.1	44.4 ±0.6	2.8 ± 0.4	6.3 ± 0.2
8	2.62 ± 0.03	588 ± 3	105.2 ± 0.1	58.3 ± 0.1	2.4 ± 0.4	4.7 ± 0.2
9	2.17 ± 0.01	379 ± 3	116.1 ± 0.1	70.7 ± 0.5	1.9 ± 0.5	4.4 ± 0.2
10	2.37 ± 0.01	426 ± 4	102.6 ± 0.1	77.5 ± 0.4	2.2 ± 0.4	4.4 ± 0.2
11	0.44 ± 0.05	623 ± 5	75.0 ± 0.3	125.6 ± 0.1	91.9 ± 0.1	4.3 ± 0.2
12	3.14 ± 0.03	502 ± 6	73.7 ± 0.3	54.7 ± 0.1	2.7 ± 0.4	3.4 ± 0.2
13	2.34 ± 0.03	456 ± 4	87.7 ± 0.3	48.1 ± 0.5	7.5 ± 0.4	5.1 ± 0.2
14	2.64 ± 0.03	486 ± 5	72.8 ± 0.2	47.2 ± 0.6	50.8 ± 0.4	4.7 ± 0.2
15	2.69 ± 0.03	548 ± 6	86.0 ± 0.1	28.9 ± 0.4	7.2 ± 0.4	4.8 ± 0.2
16	2.47 ± 0.03	300 ± 3	64.9 ± 0.3	76.2 ± 0.4	17.9 ± 0.4	4.4 ± 0.2
mean	2.45	499	89.1	62.7	13.3	4.3
median	2.42	475	86.8	58.9	4.1	4.4
max	9.00	656	137.3	125.6	91.9	6.3

For Zn and Mn the mean values were 864.3 and 1176 µg/L, respectively. The content of Zn and Mn could be influenced by agricultural practices or by metal containers used during ageing stages. White wine from Orahovac has high content of Zn compared to other samples (4413.0 µg/L). It can be explained with long contact of the equipment and wine during the process of vinification, as well as with the use of pesticides in agricultural practices (Greenough et al., 2005). The variation of Cu content in wine samples is relatively high (Table 5), ranged from 28 µg/L (sample 15) to 1108 µg/L

(sample 7), red wine from Gračanica Monastery winery and red wine from Velika Hoča, respectively. This may originate mainly from Cu accumulation in soil of using Bordeaux mixture or other copper-based fungicides (Ražić & Onjia, 2010). We do not have information on whether the used Bordeaux mixture, but assume it is used because it is the most common tool used in agriculture. Copper can also be found in the wines from the use of equipment based on this metal (Ivanova-Petropulos et al., 2013).

Table 5. Results of trace elements composition in wine samples.

µg/L	Ba	Cd	Co	Cr	Se	Ni	Pb	Mn	Cu	Zn	V
1	159.6 ±0.1	2.15 ±0.03	0.02 ±0.02	6.06 ±0.03	0.83 ±0.02	133.1 ±0.4	45.3 ±0.8	1389 ±6	686 ±6	712.9 ±0.5	0.82 ±0.02
2	111.1 ±0.1	13.51 ±0.03	4.59 ±0.06	5.26 ±0.02	0.20 ±0.02	101.3 ±0.4	54.6 ±0.8	1845 ±5	338 ±6	146.5 ±0.5	5.08 ±0.02
3	124.1 ±0.1	1.67 ±0.03	2.07 ±0.02	6.23 ±0.03	0.86 ±0.02	94.8 ±0.4	93.1 ±0.8	881 ±9	194 ±6	153.5 ±0.5	2.31 ±0.02
4	38.6 ±0.1	1.42 ±0.03	0.59 ±0.08	3.59 ±0.02	1.29 ±0.02	68.0 ±0.4	28.4 ±0.8	761 ±7	170 ±6	710.3 ±0.5	0.67 ±0.02
5	40.1 ±0.1	1.94 ±0.03	2.32 ±0.06	5.26 ±0.02	0.89 ±0.02	59.1 ±0.4	50.7 ±0.8	1051 ±6	235 ±6	4413.0 ±0.5	0.77 ±0.02
6	60.0 ±0.1	1.01 ±0.03	4.26 ±0.02	7.23 ±0.01	1.21 ±0.02	44.0 ±0.4	52.1 ±0.8	750 ±6	60 ±6	596.2 ±0.5	0.02 ±0.02
7	86.8 ±0.1	1.69 ±0.03	1.96 ±0.02	10.32 ±0.02	2.60 ±0.02	56.9 ±0.4	133.4 ±0.8	1405 ±5	1108 ±6	822.7 ±0.5	1.22 ±0.02
8	101.8 ±0.1	1.42 ±0.03	3.04 ±0.02	6.89 ±0.04	1.56 ±0.02	60.4 ±0.4	39.1 ±0.8	1360 ±5	351 ±6	765.3 ±0.5	0.86 ±0.02
9	94.8 ±0.1	1.86 ±0.03	2.09 ±0.03	6.85 ±0.04	1.30 ±0.02	75.6 ±0.4	64.3 ±0.8	1365 ±6	88 ±6	604.2 ±0.5	0.02 ±0.02
10	92.4 ±0.1	1.83 ±0.03	0.47 ±0.06	8.98 ±0.04	0.27 ±0.02	66.5 ±0.4	45.6 ±0.8	1246 ±6	64 ±6	2381.0 ±0.5	0.56 ±0.02
11	128.3 ±0.1	3.03 ±0.03	0.04 ±0.02	3.74 ±0.02	0.20 ±0.02	26.8 ±0.4	59.6 ±0.8	755 ±8	312 ±6	284.4 ±0.5	2.39 ±0.02
12	90.9 ±0.1	1.45 ±0.03	3.64 ±0.02	17.61 ±0.02	0.20 ±0.02	87.5 ±0.4	30.8 ±0.8	1422 ±3	29 ±6	181.5 ±0.5	4.96 ±0.02
13	129.8 ±0.1	1.21 ±0.03	5.11 ±0.03	14.49 ±0.02	0.18 ±0.02	98.2 ±0.4	26.7 ±0.8	1257 ±6	65 ±6	258.1 ±0.5	1.75 ±0.02
14	170.6 ±0.1	1.66 ±0.03	6.65 ±0.03	5.57 ±0.02	0.20 ±0.02	76.0 ±0.4	56.4 ±0.8	1313 ±6	45 ±6	35.8 ±0.5	0.02 ±0.02
15	76.1 ±0.1	5.33 ±0.03	3.33 ±0.02	12.31 ±0.02	2.26 ±0.02	31.0 ±0.4	78.1 ±0.8	989 ±6	28 ±6	419.3 ±0.5	0.89 ±0.02
16	49.5 ±0.1	7.60 ±0.03	2.63 ±0.02	7.41 ±0.02	0.05 ±0.02	54.6 ±0.4	145.9 ±0.8	1024 ±5	124 ±6	1345.0 ±0.5	1.19 ±0.02
mean	97.2	3.05	2.85	7.99	1.11	70.9	62.7	1176	205	864.4	1.81
median	93.6	1.76	2.63	6.87	1.05	67.2	53.3	1252	106	600.2	1.19
max	170.6	13.5	6.65	17.61	2.60	133.1	145.9	1845	1108	4413	5.09
min	38.6	1.01	0.02	3.59	0.05	26.8	26.7	750	28	35.8	0.56
sd	39.3	3.28	1.82	3.90	0.78	27.6	34.7	305	265	1107	1.54

CONCLUSION

In summary, for the first time characterization of wine samples from this region was given. It is shown that these wines are rich with polyphenols, especially cultivar Vranac, often presented in this region as variety for domestic, small wine producers. This region could be also favorable for the autochthones cultivars such as Župljanka (white wine) and Prokupac (red wine) which results shows higher content of important nutrients compared with these wines from other Balkan regions. Quality data of wines produced in this historically important viticulture region could significantly contribute to the nowadays development, certification and commercialization of wines bearing in mind that existing small private wineries and wine producers which produce high-quality wine mainly have domestic or local significance and rarely place their wines in the European markets.

ACKNOWLEDGMENTS

Financial support for this study was granted by the Ministry of Science and Technological Development of the Republic of Serbia, Agreement No. 451-03-68/2022-14/200123. The authors are grateful to families Manitašević, Garić, Stašić, Dedić, Micić, Djuričić, Večević, Nisić, Ćurčić and to P. Filijović for helping to prepare this work.

REFERENCES

Atanacković, M., Petrović, A., Jović, S., Bukarica, L. G., Bursać, M. & Cvejić, J. 2012. Influence of winemaking techniques on the resveratrol content, total phenolic content and antioxidant potential of red wines. Food Chem. 131, pp. 513-518. doi.org/10.1016/j.foodchem.2011.09.015

Babincev Lj. M., Gurešić D. M. & Simonović R. M. 2016. Spectrophotometric characterization of red wine color from the vineyard region of Metohia, Journal of Agricultural Sciences Belgrade 61(3), pp. 281-290. https://doi.org/10.2298/JAS1603281B

Cavuldak, O. A., Anli, R. E. & Vural, N. 2013. Phenolic Composition and Antioxidant Capacity of Some Red Wines from Turkey. International Journal of Food Science and Nutrition Engineering 3(3), pp. 40-47. DOI:10.5923/j.food.20130303.04

Đurđić, S., Pantelić, M., Trifković, J., Vukojević, V., Natić, M., Tešić, Ž. & Mutić, J. 2017. Elemental composition as a tool for the assessment of type, seasonal variability, and geographical origin of wine and its contribution to daily elemental intake. RSC Advance, 7, pp. 2151-2162. http://doi.org/10.1039/C6RA25105F

Geana, I., Iordache, A., Ionete, R., Marinescu, A., Ranca, A. & Culea, M. 2013. Geographical origin identification of Romanian wines by ICP-MS elemental analysis. Food Chemistry, 138, pp. 1125-1134. DOI:10.1016/j.foodchem.2012.11.104

Greenough, J. D., Mallory-Greenough, L. M. & Fryer, B. J. 2005. Geology and Wine 9: Regional Trace Element Fingerprinting of Canadian Wines. Geoscience Canada, 32(3), pp. 129-137. https://journals.lib.unb.ca/index.php/GC/article/view/2712

Iglesias, M., Besalu E. & Anticó, E. 2007. Internal Standardization−Atomic Spectrometry and Geographical Pattern Recognition Techniques for the Multielement Analysis and Classification of Catalonian Red Wines. J. Agric. Food Chem., 55, pp. 219-225. https://doi.org/10.1021/jf0629585

Ivanišević, D. & Jakšić, D. 2012. Viticulture in Serbia according to statistics and viticulture zoning, Final Conference, Application Census of Agriculture 2012 in the situation of agriculture and in the planning of agricultural policy in the Republic of Serbia. http://media.popispoljoprivrede.stat.rs/2014/Dokumenta/Radovi/Viticulture%20in%20Serbia%20according%20to%20statistics%20and%20viticulture%20zoning.pdf

Ivanova, V., & Stefova, M. 2010. Chinnici, F. Determination of the polyphenol contents in Macedonian grapes and wines by standardized spectrophotometric methods. J. Serb. Chem. Soc., 75(1), pp. 45-59. https://doi.org/10.2298/JSC1001045I

Ivanova-Petropulos, V., Wiltsche, H., Stafilov, T., Stefova, M., Motter, H., & Lankmayr, E. 2013. Multielement analysis of Macedonian wines by inductively coupled plasma–mass spectrometry (ICP-MS) and inductively coupled plasma–optical emission spectrometry (ICP-OES) for their classification. Macedonian Journal of Chemistry and Chemical Engineering, 32(2), pp. 265-281. DOI:10.20450/mjcce.2013.447

Katalinić, V., Milos, M., Modun, D., Musić, I. & Boban, M. 2004. Antioxidant effectiveness of selected wines in comparison with (+)-catechin. Food Chem., 86, pp. 593-600. https://doi.org/10.1016/j.foodchem.2003.10.007

Menković, N., Živković, J., Šavikin, K., Gođevac, D., Zdunić, G., 2014. Phenolic composition and free radical scavenging activity of wine produced from the Serbian autochthonous grape variety Prokupac – A model approach. J. Serb. Chem. Soc. 79(1), pp. 11-24. https://doi.org/10.2298/JSC130511089M

Pisoschi, A. M. & Negulescu, G. P. 2011. Methods for Total Antioxidant Activity Determination. A Review, Biochem & Anal Biochem, 1, pp. 1-10. DOI: 10.4172/2161-1009.1000106

Pohl, P. 2007. What do metals tell us about wine? Trends in Analytical Chemistry, 26(9), pp. 941-949. https://doi.org/10.1016/j.trac.2007.07.005

Rastija, V. & Medić-Šarić, M., 2009. Chromatographic Methods for the Analysis of Polyphenols in Wines. Journal of Chemists and Chemical Engineers, 58(03), pp. 121-128. https://hrcak.srce.hr/32964

Ražić, S. & Onjia, A. 2010. Trace element analysis and pattern recognition techniques in classification of wine from central Balkan countries. American Journal of Enology and Viticulture (ASEV) 61(4), pp. 506-511. DOI: 10.5344/ajev.2010.10002

Rodrigues, S. M., Otero, M., Alves, A. A., Coimbra, J., Coimbra, M. A., Pereira, E. & Duarte A. C. 2011. Elemental analysis for categorization of wines and authentication of their certified brand of origin. J. Food Compos.Anal.24,pp. 548-562. DOI: 10.1016/j.jfca.2010.12.003

Šeruga, M., Novak, I. & Jakobek, L. 2011. Determination of polyphenols content and antioxidant activity of some red wines by differential pulse voltammetry, HPLC and spectrophotometric methods . Food Chem. 124, pp. 1208-1216. https://doi.org/10.1016/j.foodchem.2010.07.047

Sánchez-Moreno, C., Larrauri, J. A. & Saura-Calixto, F. 1999. Free radical scavenging capacity of selected red, rose and white wines. J. Sci. Food Agric., 79, pp. 1301-1304. https://doi.org/10.1002/(SICI)1097-0010(19990715)79:10<1301::AID-JSFA367>3.0.CO;2-Y

Stafilov, T. & Karadjova I. 2006. Methods for determination and speciation of trace elements in wine (review). International Journal of Pure and Applied Chemistry (IRJPAC),1,2, pp. 273-305. http://hdl.handle.net/20.500.12188/13830

Stratil P, Kuban V. & Fojtova J. 2008. Comparison of the phenolic content and total antioxidant activity in wines as

determineted by spectrophotometric methods. Czech J. FoodSci.26, pp. 242-253. https://www.agriculturejournals.cz/publicFiles/01961.pdf

Thiel G. & Danzer Fresenius K. 1997. Direct analysis of mineral components in wine by inductively coupled plasma optical emission spectrometry (ICP-OES). J. Anal. Chem. 357, pp. 553-557. https://doi.org/10.1007/s002160050212

Vinković Vrček I., Bojić M., Žuntar I., Mendaš G. & Medić-Šarić M. 2011. Phenol content, antioxidant activity and metal composition of Croatian wines deriving from organically and conventionally grown grapes. Food Chem. 124, pp. 354-361. https://doi.org/10.1016/j.foodchem.2010.05.118

Waterhouse A., Folin-Ciociocalteu micro method; Department of Viticulture and Enology; University of California, Davis. https://waterhouse.ucdavis.edu/folin-ciocalteau-micro-method-total-phenol-wine

Bulletin of Natural Sciences Research
Vol. 12, No. 2, 2022, pp. 14-19.

DOI: https://doi.org/10.5937/bnsr12-39990
Original Scientific Paper

GEOSPATIAL ASSESSMENT OF VEGETATION CONDITION PRE-WILDFIRE AND POST-WILDFIRE ON LUŠTICA (MONTENEGRO) USING DIFFERENCED NORMALIZED BURN RATIO (DNBR) INDEX

FILIP VUJOVIĆ[1*], GOJKO NIKOLIĆ[1]

[1]Department of Geography, Faculty of Philosophy, University of Montenegro, Nikšić, Montenegro

ABSTRACT

Wildfire is one of the most dangerous environmental stressors in most vegetation zones worldwide. Determining and monitoring this stressor is important because of the disturbances that occur during the burning of biomass in ecosystems, as well as because of the damage or suffering of organisms. In the last decade, a greater number of wildfires and burnt areas were recorded in Southern Europe and Montenegro. Therefore, it is important to develop optimal methodology and models to help in better management of forest protection against wildfire. The spatial component in firefighting plays a significant role in management. In this context, Remote Sensing and Geographic Information Systems (GIS) come to the fore, which analyze spatial data and turn it into useful information - models applied in practice. The study aims to geospatial assess condition of vegetation pre-wildfire and post-wildfire in study area of the Luštica peninsula in Montenegro during the summer of 2017. Open and publicly available Sentinel 2 satellite was used. The scaled index differenced Normalized Burn Ratio (dNBR) of burned vegetation was applied as an indicator for assessing the state of vegetation after a wildfire in the open source software Quantum GIS (QGIS). The results of the damage assessment of the burned area based on the applied scaled index reveal that the category of low severity occupies an area of 335.86 ha (7%), moderately-low severity 250.13 ha (5%), moderately-high severity 406.22 ha (8%), high severity 238.03 ha (5%). The unburned areas occupy an area of 3624.95 ha (75%). This study contributes to assessing vegetation conditions and other accompanying activities pre-wildfire and post-wildfire using modern open-source geospatial tools.

Keywords: Wildfire, GIS, Remote sensing, Burned vegetation, Montenegro.

INTRODUCTION

Wildfire (Pavelek et al., 2017) or wildland fire (Eskandari, 2017) burns without control in a natural environment where the main and primary fuel is vegetation (Marić et al., 2021).

Wildfire is the one of most hazardous natural disasters (Bonazountas et al., 2005). It is also one of the most dangerous environmental stressors today. It is a significant disorder where a large part of the biomass is combusted and burned, and due to intensive exposure to heat and toxicity, organisms can be killed or damaged (Freedman, 2015; Potić et al., 2017).

Their impact on the physical and biological environment is hard to underestimate; they affect land use and land cover, ecosystems, biodiversity, natural disasters and contemporary climate change. As such, they influence and somewhat determine the socio-economic system of the areas in which they appear (Lukić et al., 2017; Adaktylou et al., 2020).

During the last decade, a large number of forest fires affected the area of southern Europe, as well as Montenegro. The previous wildfire protection system in Montenegro, especially in the coastal region of Montenegro, was inadequate. Given that it does not produce results, one could safely conclude that it is dysfunctional (Ministry of the Interior of Montenegro, 2021).

Therefore, it is important to develop optimal methodology and models to help in better management of forest protection against wildfire. The spatial component in firefighting plays a significant role in management. In this context, Remote Sensing and Geographic Information Systems (GIS) come to the fore, which analyze spatial data and turn it into useful information - models applied in practice (Valjarević & Živković, 2016; Jovanović et al., 2018; Potić & Šimunić, 2019; Milanović et al., 2009, 2016, 2019, 2020; Šiljeg et al., 2017, 2021 Artan & Spalević, 2020; Durlević et al., 2021; Ćurić et al., 2022).

Remote sensing enables the use of various tools, which with the help of recordings from several periods ensure users the identification of changes and the quantification of losses after wildfire. Due to their high spatial (10 m) and temporal (5 days) resolutions, the time series of images of the Copernicus satellite SAR Sentinel 1 (S-1) and the optical Sentinel 2 (S-2) provide a great opportunity to monitor vegetation areas. Unlike most SAR data (e.g. RADARSAT-2 or TerraSAR-X) and optical satellite platforms (e.g. SPOT, Planet, WorldView 2,3) this data is free and available for use without restrictions (Jovanović et al., 2021).

*Corresponding author: vujovicfilip@hotmail.com

The application of Normalized Burn Ratio (NBR) and differenced Normalized Burn Ratio (dNBR) indices using satellite images has been the subject of many studies in various wildfire-affected landscape areas and is considered to be effective for identifying damage to burned areas (Roy et al., 2006; Miller & Thode, 2007; Keeley, 2009; Veraverbeke et al., 2010; Parker et al., 2015; Potić et al., 2016, 2017, 2019; Jovanović & Župan 2017; Santos et al., 2020; Alcaras et al., 2022; Ponomarev et al., 2022).

This study aims to geospatial assess condition of vegetation pre-wildfire and post-wildfire in study area of the Luštica peninsula in Montenegro during the summer of 2017. Open and publicly available Sentinel 2 satellite data were used. The scaled index dNBR of burned vegetation was applied as an indicator for assessing the state of vegetation after a wildfire in GIS open-source software Quantum GIS (QGIS).

MATERIALS AND METHODS

Study area

This study was conducted for the area of the Luštica peninsula (Figure 1), which is located in the coastal area of Montenegro at the entrance to the Bay of Kotor (42°21′42″ - 42°25′55″ N, 18°32′50″ - 18°42′36″ E). It covers an area of 48 km^2. The territory of the peninsula belongs to the municipalities of Tivat and Herceg Novi. The most widespread is the karst type of relief formed by banked and layered limestones, and less often dolomite, in the central part it has the character of an undulating plain with several scarps, sinkholes and coves. The coast is characterized by numerous bays, cliffs, capes and coves with several beaches. The climate has all the characteristics of the Mediterranean.

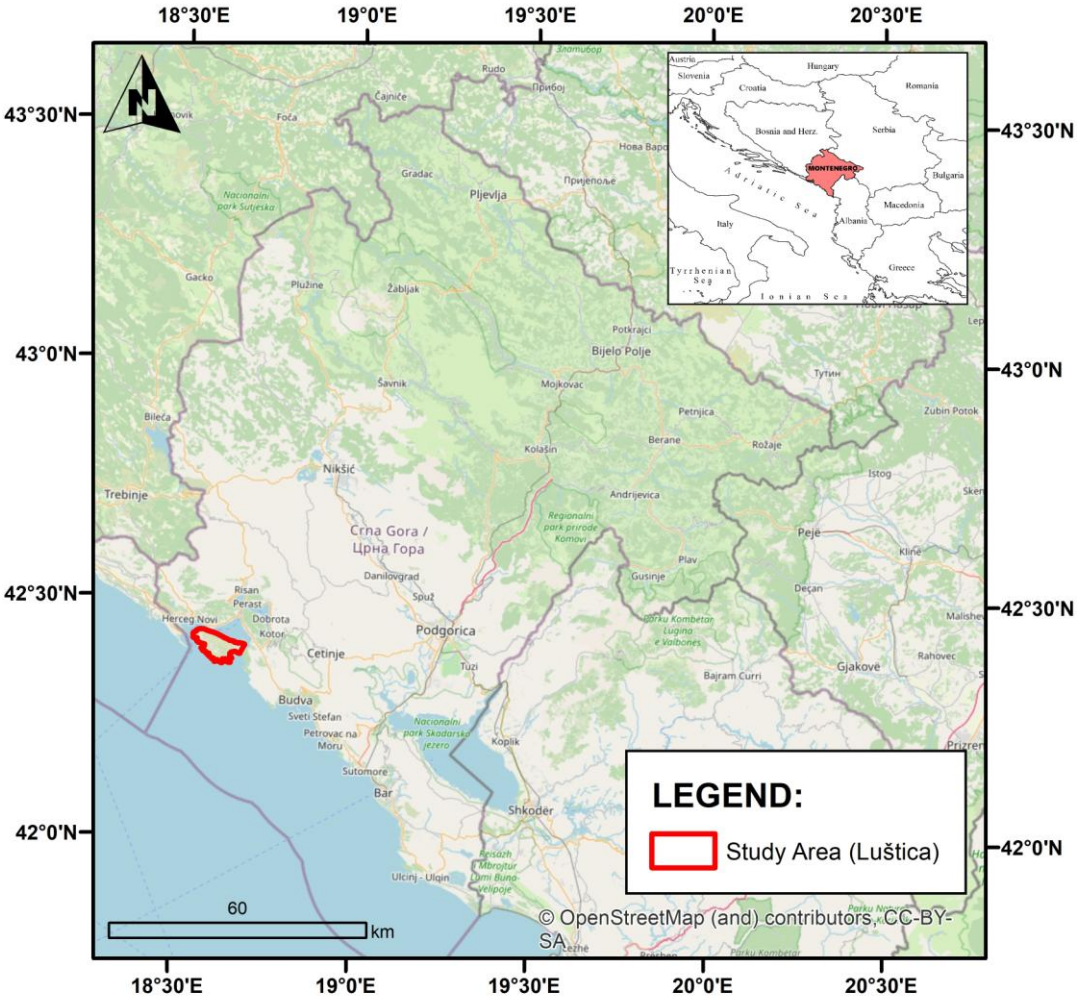

Figure 1. Location map of Luštica.

Typical Mediterranean vegetation has developed on Luštica. Maquis is the dominant type of vegetation. A set of specific and varied natural and cultural landscapes (Figure 2) characterizes the entire geospace making a unique and harmonious whole of natural, semi-natural, cultural and recognizable remains of olive cultivated area (Čurović et al., 2019).

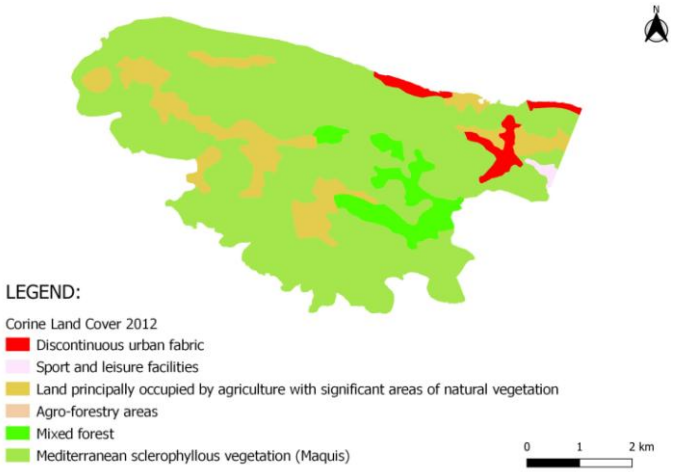

Figure 2. Landscape map according to CLC 2012.

Input data

Open-source and free-of-charge Sentinel-2 satellite images are provided by ESA (European Space Agency) through the constellation of Sentinel-2A and Sentinel-2B satellites. For this study, images from the Sentinel-2A satellite are used. Band characteristics with resolution and central wavelengths are found in Table 1. The Copernicus program continuously monitors the Earth through Sentinel satellites. These satellite images from the geospatial database are the main data acquisition channel for risk and recovery mapping (ESA, 2015).

For the purposes of this study, two Sentinel-2A data sets were used: the first data set refers to July 14, 2017, and represents the pre-wildfire scenario. While the second one was acquired on August 23, 2017, and represented the scenario post-wildfire.

Methodology

Geospatial modeling process of selected Sentinel-2A images for geospatial assessment of vegetation condition pre-wildfire and post-wildfire implemented in open-source GIS software Quantum GIS (QGIS) 3.18.2.

Both images were resampled using the cubic convolution method, so they are oriented towards the north and georeferenced projection coordinate system of the universal transverse Mercator projection (UTM 34N) on the WGS84 rotation ellipsoid (EPSG:32634) and stored in raster GeoTIFF format. The images are cropped within the boundaries of the Luštica peninsula for easier further processing using tool Extract by Mask.

The Normalized Burn Ratio (NBR) was developed to help identify areas affected by wildfire and assess the damage to those areas (Equation 1) (García & Caselles, 1991). The Differenced NBR (dNBR) is a scaled index of the magnitude of changes caused by wildfire in a certain area and is used as a descriptive measure of environmental change (Equation 2) (Key & Benson, 1999, 2004; Twele, 2004). Finally, the NBR and dNBR were calculated in Raster Calculator using expressions:

$$NBR = \frac{(NIR - SWIR)}{(NIR + SWIR)} \quad (1)$$

$$dNBR = NBR_{pre} - NBR_{post} \quad (2)$$

Obtained raster values after implementation expressions were reclassified according to the standardized dNBR categories from Table 2 for easier quantitative and visual interpretation of the results using Reclassify by Table tool. After that, the reclassified raster values were converted to a vector using Raster to Polygon tool for calculation of the area for the categories. In the end, the areas were calculated for all categories in Attribute Table in Field Calculator.

Table 1. Features of Sentinel-2A images.

Sentinel-2A		
Band	Central Wavelength (μm)	Resolution (m)
B1-Coastal Aerosol	0.443	60
B2-Blue	0.490	10
B3-Green	0.560	10
B4-Red	0.665	10
B5-Red Edge1	0.705	20
B6-Red Edge2	0.740	20
B7-Red Edge3	0.783	20
B8-NIR	0.842	10
B8A-Narrow NIR	0.865	20
B9- Water Vapor	0.945	60
B10-SWIR Cirrus	1.375	60
B11-SWIR1	1.610	20
B12-SWIR2	2.190	20

*Source: ESA, 2015

Table 2. Value range of the dNBR to classify fire severity.

dNBR value range	Wildfire severity
<0.099	Unburned
0.100 - 0.269	Low severity
0.270 - 0.439	Moderate-low severity
0.440 - 0.659	Moderate-high severity
>0.660	High severity

*Source: ESantos et al., 2020; Ponomarev et al., 2022

RESULTS

The results of geospatial assessment reveal (Table 3) that the dNBR category of low severity occupies an area of 335.86 ha (7%), moderately-low severity 250.13 ha (5%), moderately-

high severity 406.22 ha (8%), high severity 238.03 ha (5%). The dNBR category of unburned areas occupy an area of 3624.95 ha (75%). In order to simplify the spatial layout and scope, an overview map was created (Figure 3).

The maximum value of dNBR for burned areas was 1.07, the minimum value was 0.100, the mean value was 0.467, and the standard deviation was 0.208. Figure 4 shows the dependence (distribution) of dNBR value of each image pixel and frequency. The most frequent value was 0.617.

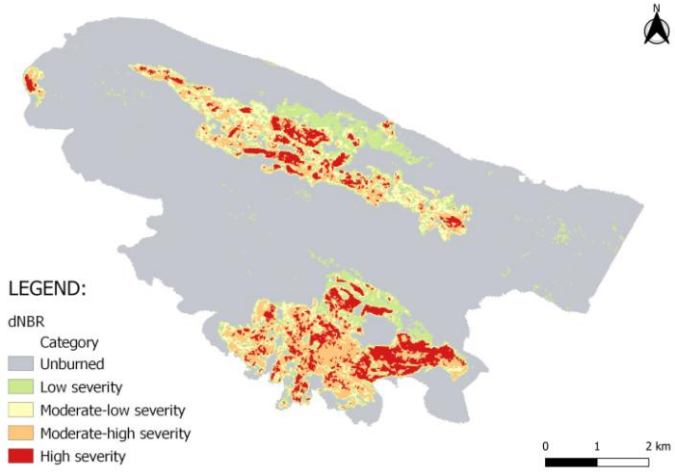

Figure 3. Overview map according to dNBR categories.

Table 3. Results according to dNBR categories.

Wildfire severity	ha	%
Unburned	3624.95	75
Low severity	335.86	7
Moderate-low severity	250.13	5
Moderate-high severity	406.22	8
High severity	238.03	5

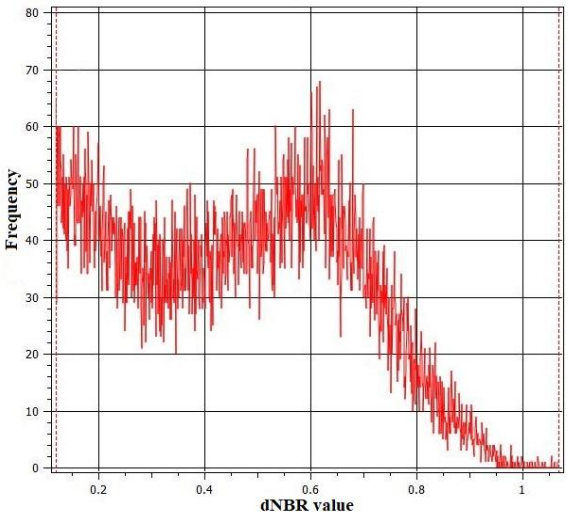

Figure 4. Graph of frequency.

DISCUSSION AND CONCLUSION

From geospatial assessment results, one can gain an insight into the harmful effects of wildfire activities on the vegetation cover. Information on vegetation condition post-wildfire in the study area can be significant for continuous monitoring of the environment and assessment of vegetation succession (Brovkina et al., 2020; Pešić et al., 2020).

This kind of geospatial assessment using the dNBR index has been validated many times in different geographical conditions, and its high efficiency has been widely discussed in previous studies (Jovanović & Župan 2017; Potić et al., 2017; Llorens et al., 2021; Alcaras et al., 2022; Ponomarev et al., 2022). This study shows the possibility of assessing vegetation's condition pre-wildfire and post-wildfire based on Sentinel-2a satellite images in a QGIS environment using the dNBR index.

There are numerous advantages of this assessment: the possibility of using it in different geographical conditions, fast research for a large area, continuous monitoring of the environment, using open-source geospatial data and software without restrictions, easy possibilities of obtaining the results of the assessment with cartographic presentation in a GIS. In addition, this approach represents an alternative to the European Forest Fire Information System (EFFIS), which uses MODIS satellite images to assess burned areas (Llorens et al., 2021). However, it is essential to say that the assessment in this study uses Sentinel-2a images that have satisfactory resolution and quality for certain applications (Jovanović et al., 2021).

Therefore, in future studies, it would be good to use satellite images of better resolution or quality in order to obtain more relevant assessment results.

This approach contributes significantly in the case of scarce geospatial tools and can be decisive for the need for sustainable and ecological management of the vegetation cover of southern Europe, which is under constant wildfire hazard in the summer.

REFERENCES

Adaktylou, N., Stratoulias, D. & Landenberger, R. 2020. Wildfire risk assessment based on geospatial open data: Application on Chios, Greece. ISPRS International Journal of Geo-Information, 9(9), pp. 516. DOI: 10.3390/ijgi9090516

Alcaras, E., Costantino, D., Guastaferro, F., Parente, C. & Pepe, M. 2022. Normalized Burn Ratio Plus (NBR+): A New Index for Sentinel-2 Imagery. Remote Sensing, 14(7), pp. 1727. DOI: 10.3390/rs14071727

Artan, H. & Spalevic, V. 2020. Testing NDVI, tree cover density and land cover type as fuel indicators in the wildfire spread capacity index (WSCI): case of Montenegro. Notulae Botanicae Horti Agrobotanici Cluj-

Napoca, 48(4), pp. 2368-2384. DOI: 10.15835/nbha48411993

Bonazountas, M., Kallidromitou, D., Kassomenos, P. A. & Passas, N. 2005. Forest fire risk analysis. Human and Ecological Risk Assessment, 11(3), pp. 617-626. DOI: 10.1080/10807030590949717

Brovkina, O., Stojanović, M., Milanović, S., Latypov, I., Marković, N. & Cienciala, E. 2020. Monitoring of post-fire forest scars in Serbia based on satellite Sentinel-2 data. Geomatics, Natural Hazards and Risk, 11(1), pp. 2315-2339. DOI: 10.1080/19475705.2020.1836037

Ćurić, V., Durlević, U., Ristić, N., Novković, I. & Čegar, N. 2022. GIS application in analysis of threat of forest fires and landslides in the Svrljiški Timok Basin (Serbia). Glasnik Srpskog geografskog drustva, 102(1), pp. 107-130. DOI: 10.2298/GSGD2201107C.

Čurović, Ž., Čurović, M., Spalević, V., Janic, M., Sestras, P. & Popović, S. G. 2019. Identification and evaluation of landscape as a precondition for planning revitalization and development of mediterranean rural settlements—Case study: Mrkovi Village, Bay of Kotor, Montenegro. Sustainability, 11(7), pp. 2039. DOI: 10.3390/su11072039

Durlević, U., Novković, I., Lukić, T., Valjarević, A., Samardžić, I., Krstić, F. et al. 2021. Multihazard susceptibility assessment: A case study–Municipality of Štrpce (Southern Serbia). Open Geosciences, 13(1), pp. 1414-1431. DOI: 10.1515/geo-2020-0314.

ESA. 2015. Sentinel-2 User Handbook. https://sentinels.copernicus.eu/documents/247904/685211/Sentinel-2_User_Handbook.pdf/8869acdf-fd84-43ec-ae8c-3e80a436a16c?t=1438278087000

Eskandari, S. 2017. A new approach for forest fire risk modeling using fuzzy AHP and GIS in Hyrcanian forests of Iran. Arabian Journal of Geosciences, 10(8), pp. 1-13. DOI: 10.1007/s12517-017-2976-2

European Environment Agency. 2020. Corine Land Cover 2012. http://land.copernicus.eu/pan-european/corine-land-cover/clc-2012/. Accessed May 20, 2022.

Freedman, B. 2015. Ecological Effects of Environmental Stressors. Oxford Research Encyclopedia of Environmental Science. DOI: 10.1007/1-4020-4494-1_94

García, M. L. & Caselles, V. 1991. Mapping burns and natural reforestation using Thematic Mapper data. Geocarto International, 6(1), pp. 31-37. DOI: 10.1080/10106049109354290.

Jovanović, D., Gavrilović, M., Borisov, M. & Govedarica, M. 2021. Uporaba Sentinel 1 i Sentinel 2 snimaka u identifikaciji nestalih šumskih površina–studija slučaja Fruška gora (Srbija). Šumarski list, 145(3-4), pp. 127-134. DOI: 10.31298/sl.145.3-4.2

Jovanović, N. & Župan, R. 2017. Analysis of Vegetation Condition before and after Forest Fires in Dalmatia using Sentinel-2 Satellite Images. Geodetski list, 71(3), pp. 233-248.

Keeley, J. E. 2009. Fire intensity, fire severity and burn severity: a brief review and suggested usage. International journal of wildland fire, 18(1), pp. 116-126.

Key, C. H. & Benson, N. C. 2004. Remote Sensing Measure of Severity: The Normalized Burn Ratio. FIREMON Landscape Assessment (LA) V4 Sampling and Analysis Methods. Collins, CO: USFS Rocky Mountain Research Station

Key, C. H., & Benson, N. C. 1999. The Normalized Burn Ratio (NBR): A Landsat TM Radiometric Index of Burn Severity. Retrieved from: https://archive.usgs.gov/archive/sites/www.nrmsc.usgs.gov/files/norock/products/SEVER36_im_copy6.pdf.

Llorens, R., Sobrino, J. A., Fernández, C., Fernández-Alonso, J. M., & Vega, J. A. 2021. A methodology to estimate forest fires burned areas and burn severity degrees using Sentinel-2 data. Application to the October 2017 fires in the Iberian Peninsula. International Journal of Applied Earth Observation and Geoinformation, 95, 102243. DOI: 10.1016/j.jag.2020.102243

Lukić, T., Marić, P., Hrnjak, I., Gavrilov, M. B., Mladjan, D., Zorn, M. & Stojsavljević, R. 2017. Forest fire analysis and classification based on a Serbian case study. Acta geographica Slovenica, 57(1), pp. 51-63. DOI: 10.3986/AGS.918

Maric, I., Siljeg, A. & Domazetovic, F. 2021. Derivation of Wildfire Ignition Index using GIS-MCDA from High-Resolution UAV Imagery Data and Perception Analysis in Settlement Sali, Dugi Otok Island (Croatia), GISTAM conference, pp. 90-97.

Milanović M., Micić T., Lukić T., Nenadović S. S., Basarin B., Filipović D.J., et al. 2019. Application of Landsat-derived NDVI in monitoring and assessment of vegetation cover changes in Central Serbia. Carpathian Journal of Earth and Environmental Sciences, 14(1), pp. 119-129. DOI: 10.26471/cjees/2019/014/064

Milanovic, M. & Ljesevic, M. 2009. Methods of Remote Sensing in Environment, University of Belgrade, Belgrade: Faculty of Geography.

Milanović, M. M., Perović, V. S., Tomić, M. D., Lukić, T., Nenadović, S. S., Radovanović, M. M., Ninković, M. M., Samardžić, I. & Miljković, Đ. 2016. Analysis of the state of vegetation in the municipality of Jagodina (Serbia) through remote sensing and suggestions for protection. Geographica Pannonica, 20(2), pp. 70–78. DOI: 10.5937/GeoPan1602070M

Milanovic, M., Valjarevic, A. & Lukic, T. 2020. Remote Sensing of Environment – Second Edition, Belgrade: Faculty of Geography.

Miller, J. D. & Thode, A. E. 2007. Quantifying burn severity in a heterogeneous landscape with a relative version of the delta Normalized Burn Ratio (dNBR). Remote Sensing of Environment, 109(1), pp. 66-80.

Ministry of Internal Affairs of Montenegro. 2021. Disaster Risk Assessment in Montenegro. Podgorica: Grafo Group D.O.O. https://www.gov.me/clanak/procjena-rizika-od-katastrofa

Parker, B. M., Lewis, T. & Srivastava, S. K. 2015. Estimation and evaluation of multi-decadal fire severity patterns using Landsat sensors. Remote Sensing of Environment, 170, pp. 340-349. DOI: 10.1016/j.rse.2015.09.014

Pavlek, K., Bišćević, F., Furčić, P., Grđan, A., Gugić, V., Malešić, N., Moharić, P., Vragović, V., Fuerst-Bjeliš, B. & Cvitanović, M. 2017. Spatial patterns and drivers of fire occurrence in a Mediterranean environment: a case study of southern Croatia. Geografisk Tidsskrift-Danish Journal

of Geography, 117(1), pp. 22-35. DOI: 10.1080/00167223.2016.1266272

Pešić, V., Kostianoy, A. G. & Soloviev, D. M. 2020. The impact of wildfires on the Lake Skadar/Shkodra environment. Ecologica Montenegrina, 37, pp. 51-65. DOI: 10.37828/em.2020.37.7

Ponomarev, E., Zabrodin, A. & Ponomareva, T. 2022. Classification of fire damage to boreal forests of Siberia in 2021 based on the dNBR index. Fire, 5(1), pp. 19. DOI: 10.3390/fire5010019

Potić, I. & Šimunić, V. 2019. Mapping of the environment using multispectral satellite imagery. The University Thought-Publication in Natural Sciences, 9(2), pp. 38-42. https://doi.org/10.5937/univtho9-24474

Potić, I. 2016. Remote sensing approach to forest fires monitoring. The Environment Environment Science and Policy for Sustainable Development, 4(2):47-51.

Potić, I. M., Ćurčić, N. B., Potić, M. M., Radovanović, M. M. & Tretiakova, T. N. 2017. Remote sensing role in environmental stress analysis: East Serbia wildfires case study (2007-2017). Journal of the Geographical Institute" Jovan Cvijic", SASA, 67(3), pp. 249-264. DOI: 10.2298/IJGI1703249P

Roy, D. P., Boschetti, L. & Trigg, S. N. 2006. Remote sensing of fire severity: assessing the performance of the normalized burn ratio. IEEE Geoscience and Remote Sensing Letters, 3(1), pp. 112-116. DOI: 10.1109/LGRS.2005.858485

Santos, S. M. B. D., Bento-Gonçalves, A., Franca-Rocha, W. & Baptista, G. 2020. Assessment of burned forest area severity and postfire regrowth in chapada diamantina national park (Bahia, Brazil) using dnbr and rdnbr spectral indices. Geosciences, 10(3), pp. 106. DOI: 10.3390/geosciences10030106

Sentinel 2, USGS EarthExplorer. 2017. Retrieved from https://earthexplorer.usgs.gov/

Šiljeg, A., Marić, I., Jurišić, M. & Plaščak, I. 2017. Viewshed model as a strategy for prevention of forest fires–case study of Zadar county. Šumarski list, 141(7-8), pp. 339-349. DOI: 10.31298/sl.141.7-8.1

Šiljeg, A., Milošević R. & Marić I. 2021. Primjena višekriterijskih GIS analiza u izvođenju indeksa rizika izbijanja otvorenih požara I optimizacija vatrogasnih intervencija na području NP Krka. Geodetski glasnik, 2, 87-108.

Twele, A. 2004. Post-fire Vegetation Regeneration: the Case Study of the "Massif De L'Etoile'" Fire. European Commission Joint Research Centre.

Valjarević, A. & Živković, D. 2016. GIS & satellite detection analyses of forest belt in Prokuplje municipality. Tehnički vjesnik-Technical Gazette, 23(4), pp. 969-972. DOI: 10.17559/TV-20140222204458

Veraverbeke, S., Lhermitte, S., Verstraeten, W. W. & Goossens, R. 2010. The temporal dimension of differenced Normalized Burn Ratio (dNBR) fire/burn severity studies: The case of the large 2007 Peloponnese wildfires in Greece. Remote Sensing of Environment, 114(11), pp. 2548-2563.

Bulletin of Natural Sciences Research
Vol. 12, No. 2, 2022, pp. 20-24.
DOI: https://doi.org/10.5937/bnsr12-40500
Original Scientific Paper

CHANGES IN THE NUMBER AND CHARACTERISTICS OF THE NATURAL INCREASE OF THE POPULATION OF GORNJE POLIMLJE IN THE SECOND HALF OF THE 20TH AND THE BEGINNING OF THE 21ST CENTURY

ĐOKO RAIČEVIĆ[1*], IVAN MIJANOVIĆ[2]

[1]Department of Geography, Tourism and Hotel Management, Faculty of Sciences, University of Novi Sad, Novi Sad, Serbia
[2]Department of Geography, Faculty of Philosophy, University of Montenegro, Nikšić, Montenegro

ABSTRACT

The northern part of Montenegro went through a very dynamic demographic development in the post-war period. The changes that have taken place can be characterised as both qualitative and quantitative, and are driven by various factors imposed by the overall social and economic development. In the second half of the 20th century, Gornje Polimlje increased the population of its towns, intensified urban development, established better social infrastructure, and achieved a more favourable openness to the surrounding countries. However, despite this, as part of north-east Montenegro it remained an underdeveloped area, which had a strong impact on the scope, intensity and quality of changes in its overall demographic development. The population of Gornje Polimlje is decreasing and the depopulation process has affected many local communities. Unfavourable demographic trends in this subregion began in the 90s of the previous century, and continued to intensify during the 21st century.

Keywords: Gornje Polimlje, Population, Population changes, Birth rate, Death rate, Natural increase.

INTRODUCTION

Gornje Polimlje is located in the northeast of Montenegro. It got its name from the fact that it covers the basin of the upper course of the river Lim. It stretches in a south-north direction, and comprises the composite Lim valley and mountains with mountain and sub-mountain parishes (Figure 1).

With its boarders, it covers an area of 1,032 km^2 (Bakić, 2005). Administratively, Gornje Polimlje consists of the following municipalities: Gusinje, Plav, Andrijevica and Berane.

Milisav Lutovac believed that Gornje Polimlje also includes Bihor, Korita up to the Kumanica Gorge, extending its borders eastward as far as Turjak. Bakić gave his objections to such borders in a paper from 2005. However, for the purposes of this paper, it was not possible to separate the population of Bihor due to the fact that the current municipality of Petnjica was part of the municipality of Berane until 2013, so the paper shows the change in the number of inhabitants as an integral part of the municipality of Berane until 2013.

The municipality of Gusinje was part of the Plav municipality until 2014, when it received the status of an independent municipality by the decision of the Government of Montenegro, following a consultative referendum.

The municipality of Andrijevica was also part of the municipality of Berane until the end of 1990, when it obtained its current status.

The movement of the total number of inhabitants of Gornje Polimlje resulted from a number of factors, in particular: the slower socio-economic transformation of the northern part of Montenegro compared to its other parts, as well as the regions in the near and far surroundings; unfavourable conditions for employment, culture and entertainment activities, and general living conditions compared to other regions of Montenegro. It should be pointed out that complete neglect of villages and the conditions for farming and living in the countryside had a significant impact on the overall demographic trends in this region (Bakić, 1994).

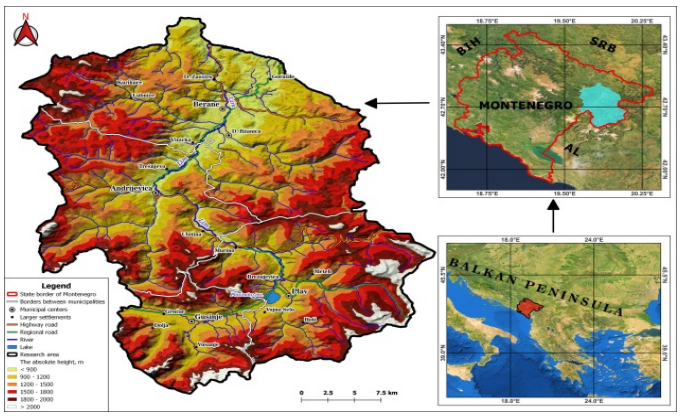

Figure 1. Geographical location of Gornje Polimlje (Source: Ivan Mijanović).

*Corresponding author: raicevicdjoko2013@yahoo.com

MATERIAL AND METHODS

Changes in the total number of inhabitants in the second half of the 20th and the first decades of the 21st century can be reliably monitored based on the results of the censuses that took place in 1953, 1961, 1971, 1981, 1991, 2003 and 2011. For the periods between censuses, vital demographic statistics of the Statistical Office of Montenegro (MONSTAT) were used for the purposes of this paper. The methodological basis consists of the usual demographic, geographic and statistical methods. Demographic and geographic methods were used during the analysis of absolute changes in the total population of Gornje Polimlje, while statistical methods will be used when processing the quantitative and qualitative results of the research. This paper aims to indicate the trends of the total number of inhabitants in the second half of the 20th century, which was examined by Bakić in his work from 2005, as a supplement to those researches, the authors presented the changes in the first decades of the 21st century, making a descriptive analysis of contradictory changes that have affected this area. For the purpose of this paper, the following indicators of the natural movement of the population will be presented: birth rate, mortality rate and natural increase rate.

RESEARCH RESULTS

Changes in the number of inhabitants in the second half of the 20th century

In the period from 1948-2021, Gornje Polimlje, i.e. the municipalities of Plav, Gusinje, Andrijevica and Berane recorded a decrease in the number of inhabitants by 11,344 or 25.9% compared to 1948.

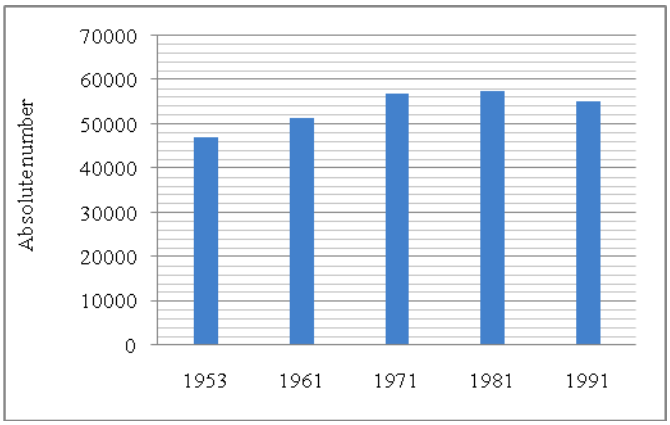

Figure 2. Number of inhabitants of Gornje Polimlje in the second half of the 20th century (Source: figure based on data: Bakić, 2005, p. 261).

Different periods exhibit different tendencies with respect to the increase and decrease of the population.

The second half of the 20th century was characterized by an upward trend, that is, an increase in the total number of inhabitants. The number of inhabitants increased from 43,753 to 55,097 in 1991.

In absolute terms, the number of inhabitants per census year ranged (Figure 2): 1953 (46,930 inhabitants); 1961 (51,276); 1971 (57,073); 1981 (57,442); 1991 (55,097) (Bakić, 2005). Compared to Montenegro, Gornje Polimlje recorded a slower growth of the total number of inhabitants in the second half of the 20th century. The growth rates in this period were: 1961/53 - 1%; 1971/61 - 0.7%; 1981/71 - 0.1%; 1991/1981 - 0.5 %. Two periods can be distinguished during this interval: the first from the second half of the 20th century until 1981, when the population increased by 13,689 inhabitants, and the second period from 1981 to 1991, when the total number of inhabitants began to decline, with Gornje Polimlje losing 2,345 inhabitants during that ten-year period. Such movements of the population are the result of mechanical movement and gradual transition from agricultural to industrial economy.

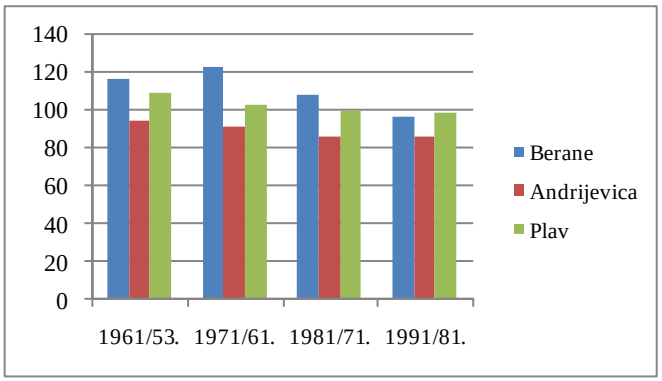

Figure 3. Vital index of the population in the municipalities of Gornje Polimlje 1953-1991 (Source: figure made on the basis of data: Bakić, 2005, p. 262).

With respect to the number of inhabitants, Berane had an upward trajectory and the number of inhabitants increased from 19,723 in 1953 to 29,096 in 1991. Population growth indices (Figure 3) in the inter-census periods for the municipality of Berane were: 1953/61 - 117; 1971/61 - 123.5; 1981/71 - 108.3; 1991/1981 - 96.4. In the second half of the 20th century, Andrijevica experienced a significant population decline, from 10,372 in 1953 to 6,696 in 1991. Andrijevica lost 35.2% of its population in this interval. Between the census years, the population movement index was: 1953/61 - 94.8; 1971/61 - 91.6; 1981/71 - 86; 1991/1981 - 86.8. In Plav, the number of inhabitants was increasing between 1953 and 1991. The number of inhabitants increased by 1,575, or by 8.8% compared to 1953. The indices ranged from: 1953/61 - 109.1; 1971/61-103.2; 1981/71 - 100.1; 1991/1981 - 98.7.

The population of Gornje Polimlje is facing complex demographic problems, which are manifested by a decrease in the birth rate. In the period from 1971-2000, birth rates were in a constant decline. In this thirty-year period, the general birth

rate decreased by 40.8%. Montenegro also features similar trends, with the birth rate decreasing by 29.7%

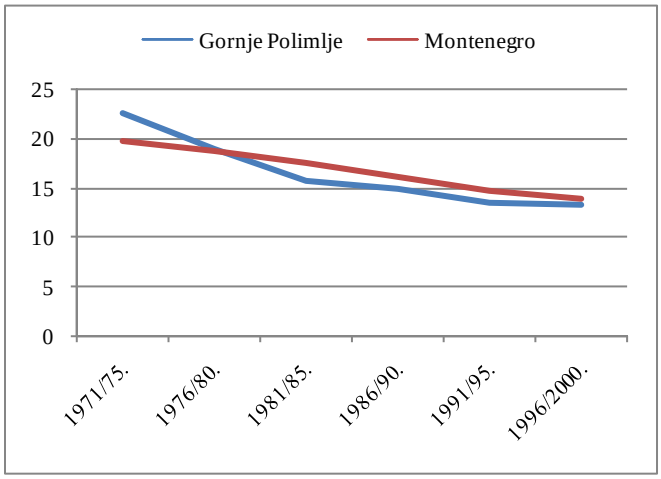

Figure 4. Changes in crude birth rate (‰) in Gornje Polimlje and Montenegro 1971-2000, (Source: figure based on data: Bakić, 2005, p. 263).

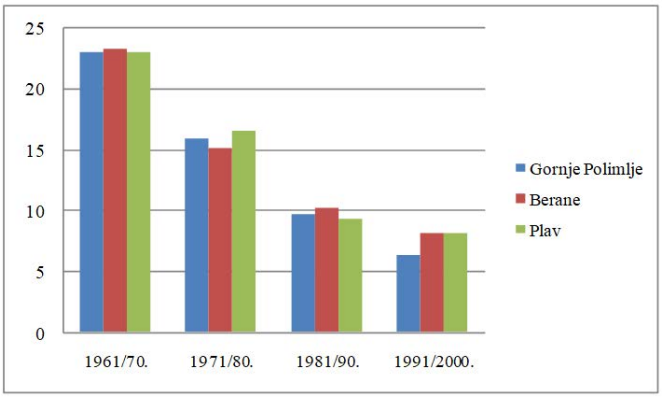

Figure 5. Natural increase (‰) in Gornje Polimlje from 1961-2000 (Source: figure based on data: Bakić, 2005, p. 265).

In the municipality of Berane[1], the general birth rate between 1971/75 stood at 22.6‰ (Plav 22.4); 1976/80 - 19.9‰ (Plav 18.1); 1981/86 - 15.9‰ (Plav 15.3); 1986/90 - 15.3‰ (Plav 14.6), 1991/96 - 14.1‰ (Plav 15.3; Andrijevica 11.2); 1996/2000 - 15.5‰ (Plav 13; Andrijevica 11.4), (Bakić, 2005).

The mortality rates of the population of Gornje Polimlje in the second half of the 20th and until the beginning of the 21st century can be characterised as low, but with a certain degree of growth. In the second half of the 20th century, mortality decreased in all age cohorts, with evident reduction in the general mortality rates of infants and children, primarily due to the improvement of the socio-economic characteristics of the population, as well as the improvement and modernisation of health care. General death rates ranged from 1971/81 - 5.4‰ (Berane 6‰, Plav 4.8‰), 1981/90 - 5.8‰ (Berane 6‰, Plav 5.4‰), 1991/2000 - 7.3‰ (Berane 6.6‰, Plav 5.9‰, Andrijevica 9.5‰).

The movement of birth and mortality rates in this period was reflected in the rates of natural increase, which were on a downward trend in the period 1961-2000 (Figure 4). Negative changes in natural increase (Figure 5) are associated with decades long decline in fertility, which manifests itself in low reproductive standards, which are accepted by an increasing number of citizens of Montenegro (Doderović & Ivanović, 2018).

Changes in the number of inhabitants during the first decades of the 21st century

The changes that took place in the second half of the 20th century continued in the first decades of the 21st century, with even greater intensity. Between 2000/21, the number of inhabitants decreased by 12,704 (Table 1). In the last two decades, this area lost an average of 604 inhabitants per year. Looking at individual municipalities, in percentage terms, the municipality of Berane lost the most inhabitants, 27.2% (9,612 inhabitants), although it cannot be said with certainty that this is relevant data, considering that until 2013, it included the municipality of Petnjica which according to the 2011. census had 5,455 inhabitants, a more realistic estimate is that Berane lost somewhere around 4,000 due to population migration, which is again a very large number. After the municipality of Berane, Andrijevica recorded the largest loss of population with 25.5% (1,511). The municipalities of Gusinje and Plav together recorded a decrease of 13.7% of inhabitants compared to 2001 (1,914). The vital index in this twenty-year period, i.e. the number of live births in relation to the number of deaths, was in a constant decline and ranged from:2002/06 - 186.1; 2006/10 -125.3; 2010/14 - 106.1; 2014/18 -99.8. In the municipality of Berane, in 2002/06 the vital index stood at 153.1 (Andrijevica 79.5; Plav 154.7; 2006/10 134.4 (Andrijevica 65; Plav 132; 2010/14 104.7 (Andrijevica 70.6; Plav 100); 2014/18 104.6 (Andrijevica 79.2; Plav 108.1; Gusinje 67). During the first two decades of the 21st century, Gornje Polimlje has been facing complex demographic problems, which are manifested by a constant decrease in the birth rate, negative natural growth, a decrease in the number of students in primary and secondary schools, an aging population, depopulation processes, emigration of the fertile and working population.

The general birth rate from 2001-2020 in the area of Gornje Polimlje, decreased by 34.1% in percentage terms, i.e. it amounted to 16.4 ‰ in 2001, while in 2020 it amounted to 10.8‰. In the mentioned time interval, there was an evident increase in general mortality rates (Figure 6), with the general mortality rate increasing by about 26%. The increase in general mortality rates can be attributed to the demographic aging of the population in this part of Montenegro, i.e. increase

[1]Andrijevica was part of the Berane municipality until the end of 1990.

of the share of old people in the total population. If we take into account the results of the natural movement of the population, it can be concluded that since 2012, there has been a constant negative natural increase, except for 2016 when it had a value of 0.6‰.

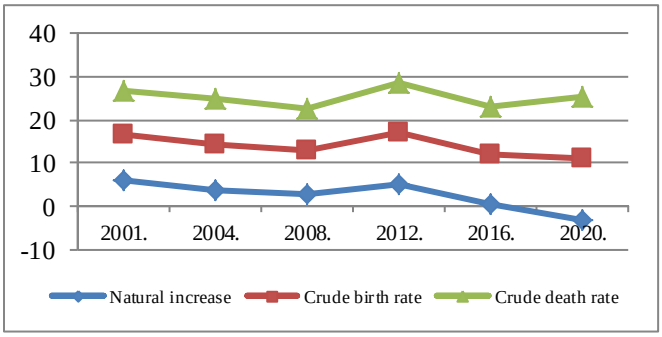

Figure 6. Natural movement of the population of Gornje Polimlje (‰) in the first decades of the 21st century (Source: figure made on the basis of vital demographic statistics available to Monstat).

Table 1. Number of inhabitants of GornjePolimlje 2000-2021.

Year	Andrijevica	Berane	Gusinje[2]	Plav	In total
2000	5914	35265	-	14127	55306
2001	5856	35086	-	13983	54925
2002	5797	34908	-	13839	54544
2003	5677	34411	-	13546	53633
2004	5737	35014	-	13813	54564
2005	5576	34516	-	13606	53699
2006	5505	34364	-	13755	53623
2007	5454	34244	-	13704	53401
2008	5395	34176	-	13671	53242
2009	5333	34038	-	13608	52979
2010	5205	34019	-	13364	52588
2011	5071	33973	-	13109	52153
2012	5041	33664	-	13006	51711
2013	5018	33353	-	12874	51245
2014	4957	27907	-	12806	45670
2015	4917	27753	3949	8799	45418
2016	4942	27513	3985	8693	45133
2017	4790	27256	3984	8628	44658
2018	4707	26903	3983	8494	44087
2019	4585	26632	3998	8319	43534
2020	4532	26393	3995	8287	43207
2021	4403	26013	3995	8191	42602

*(Source: Monstat)

[2]Gusinje was part of the municipality of Plav until 2014.

Looking at individual towns with respect to the natural movement of the population in the period from 2001 to 2020, we can notice various disproportions in their trends. The highest birth rate was recorded in the municipality of Plav in 2001 at 16 ‰, while the lowest birth rate was recorded in Gusinje in 2018 at 6.3‰. In terms of mortality, the highest value was recorded by Andrijevica with 15.5‰ in 2019, and the lowest in Plav in 2005 with 8.7‰. In the municipality of Berane, which is the largest in terms of population, the birth rate decreased by 22.3% and the mortality rate increased by 19.8% over two decades, and during this time interval, the birth rate in Andrijevica decreased by 37.3%, while the mortality rate increased by 14.8%.

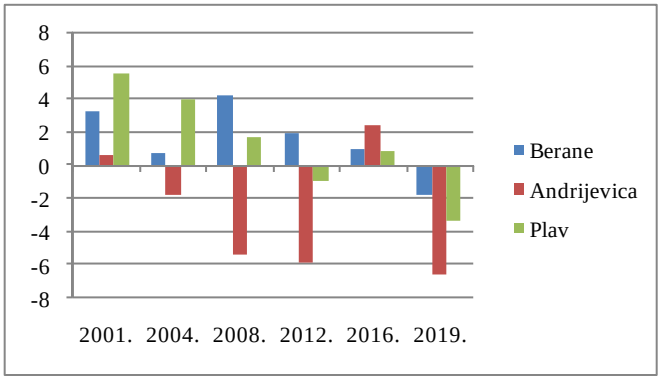

Figure 7. Rate of natural increase (‰) in the towns of Gornje Polimlje, (Source: figure based on Monstat data).

Plav is characterized by a downward trend of general birth rates amounting to 30.6%, and an increase in mortality by 38.4%. Such birth and mortality trends affected the natural increase rates, which was manifested as negative in all municipalities of Gornje Polimlje in 2019. (Figure 7).

CONCLUSION

In addition to population dynamics, the gender and age structure and its changes over time represent one of the basic characteristics of the demographic development of every country. Having this in mind, it should be pointed out that the changes in the gender and age composition of the population of Gornje Polimlje in the second half of the 20th century were influenced, primarily by the decline in fertility, but were also strongly influenced by the inherited age structure. Namely, the consequences of disturbances in the gender and age structure caused by large human losses in the First and Second World War, the sudden increase in fertility during the early 1950s, and the subsequent relatively rapid decrease in the birth rate, were the main factors that shaped the age pyramids of the population of Gornje Polimlje almost during the entire second half of the 20th century.

The projection of future demographic processes and structures has entirely practical reasons. The negative trend of

natural changes in Gornje Polimlje over the first decades of the 21st century is characterized by: a drop in birth rate, total fertility rate, net reproduction and natural increase, all below the level necessary for simple renewal of population. There is an increase in the overall mortality rate of the population, with a decrease in the mortality rate of infants and children aged 1-4 years. There are ongoing negative migration flows, especially when it comes to the younger fertile population from rural to urban settlements, and from the Northern region (which includes Gornje Polimlje) to the Central and Southern regions.

REFERENCES

Bakić, R. 2005. Gornje Polimlje: priroda, stanovništvo i naselja, Geografski institute Filozofskog fakulteta; Nikšić.

Doderović, M. & Ivanović, Z. 2018. Stanovništvo Crne Gore, MATICA br. 74, pp. 121-140.

Bakić, R. 1994. Demografski razvitak sjeverne Crne Gore, UNIREKS Nikšić.

Zavod za statistiku Crne Gore, MONSTAT. Vitalna statistika 1961-2020.godine, Podgorica.

Bulletin of Natural Sciences Research
Vol.12, No.2, 2022. pp. 25-30.

DOI: https://doi.org/10.5937/bnsr12-39725
Original Scientific Paper

NEW PROOF OF AHLFORS LEMMA ABOUT GREEN STOKES FORMULA FOR DISTRIBUTIONS

ANA SAVIĆ[1,⋆]

School of Electrical and Computer Engineering, Academy of Technical and Art Applied Studies, Belgrade, Serbia

ABSTRACT

The paper presents a new proof of Ahlfors lemma about Green Stokes formula for distributions. The proof is performed directly using test functions instead of using convolutions.

Keywords: Convolutions, Distributions, Green Stokes formula, Test functions.

INTRODUCTION

The paper presents a new proof of Ahlfors lemma about Green Stokes formula for distributions (Ahlfors, 2006). The new proof is performed directly using test functions instead of using convolutions.

If there is interest in solving the equation

$$f_{\bar{z}} = \mu f_z \tag{1}$$

where $\|\mu\|_\infty \leqslant k < 1$, Arsenović et al. (2012); Arsenović & Mateljević (2021) let's treat at the beginning the case where μ has compact support so that f will be analytic at ∞. The fixed exponent $p > 2$ will be used, such that $kC_p < 1$.

Theorem 1. If μ has compact support there exist a unique solution f of (1) such that $f(0) = 0$ and $f_z - 1 \in L_p$.

According to Theorem 1 following conclusion can be made:

Lemma 1. $\|g_z - f_z\|_p \to 0$ and $g \to f$ uniformly on compact sets.

In order to show that f has derivatives if μ has, a slight generalization of Weyl's lemma is made:

Lemma 2. If p and q are continuous and have locally integrable distributional derivatives that satisfy $p_{\bar{z}} = q_z$, then there exists a function $f \in C^1$ with $f_z = p$ and $f_{\bar{z}} = q$. (Ahlfors, 2006)

Such results are useful in deriving solutions of Beltrami's equation (1). One method, which works in higher dimensions as well is to use convolutions, see (Arsenović at al., 2021). Here we work directly with test functions. A very concise presentation is given in (Ahlfors, 2006).

The new proof of Lemma 2 will be performed directly using test functions.

In the first part of the paper, Lemma 3, Lemma 4 and Lemma 5 with their proofs are presented. Cantor's theorem on uniform continuity (Carleson & Jones, 1992), Fubini's theorem (Arsenović at al., 2012), (Mateljević, 2013a, 2012, 2013b) and the Mean value theorem (Duren, 2004) were used in the proofs.

Below are given Theorem 2 and Theorem 3 with proofs, which represent a new proof of Ahlfors lemma about Green Stokes formula for distributions. A new proof is provided directly using test functions instead of using convolutions.

THEORETICAL PART

Let $F : \mathbb{R} \longrightarrow \mathbb{R}$ be defined as

$$F(t) = \begin{cases} e^{-1/t}, & t > 0. \\ 0, & t \leqslant 0. \end{cases} \tag{2}$$

Lemma 3. The function F is infinitely differentiable. Let C be a set of all functions $f : \mathbb{R} \longrightarrow \mathbb{R}$ such that there exists a real rational function r such that we have

$$f(t) = \begin{cases} r(x)e^{-1/t}, & t > 0. \\ 0, & t \leqslant 0. \end{cases} \tag{3}$$

Let f be an arbitrary function from the C class. Then it holds that

$$\lim_{t\to 0+} f(t) = \lim_{t\to 0+} \frac{r(t)}{e^{1/t}} = \lim_{x\to\infty} \frac{r(1/x)}{e^x} = 0 = f(0), \tag{4}$$

so the function f is continuous. It also holds that

$$\lim_{t\to 0+} \frac{f(t) - f(0)}{t} = \lim_{t\to 0+} \frac{f(t)}{t} = \lim_{t\to 0+} \frac{r(t)}{t\, e^{1/t}} = \lim_{x\to\infty} \frac{x\, r(1/x)}{e^x} = 0, \tag{5}$$

so the function f is differentiable and we have

$$f'(t) = \begin{cases} (r(t)' + r(t)/t^2)e^{-1/t}, & t \geq 0. \\ 0, & t \leqslant 0. \end{cases} \tag{6}$$

Hence it follows that $f' \in C$.

It follows in particular that the functions from the C class are differentiable and that the class C is closed for derivatives. It clearly implies that all functions from the class C are infinitely differentiable. In particular, it holds that F is infinitely differentiable.

Let $\varepsilon > 0$. Since the function $x \mapsto F(\varepsilon^2 - x^2)$ is indefinitely differentiable and positive on the interval $(-\varepsilon, \varepsilon)$, and equals zero outside it, its integral in $\mathbb{R}$ is finite and positive, and the C_ε constant can be defined as

$$C_\varepsilon = (\int_{\mathbb{R}} F(\varepsilon^2 - x^2)\, dx)^{-1}. \tag{7}$$

Let us define the function $\omega_\varepsilon : \mathbb{R} \longrightarrow \mathbb{R}$ with $\omega_\varepsilon(x) = C_\varepsilon F(\varepsilon^2 - x^2)$. It is infinitely differentiable, non-negative and it holds that $\int_{\mathbb{R}} \omega_\varepsilon(x)\, dx = 1$.

⋆ Corresponding author: ana.savic@viser.edu.rs

Let us define the function $\mu_\varepsilon : \mathbb{R} \longrightarrow \mathbb{R}$ in the following way: $\mu_\varepsilon(x) = \int_0^x \omega_{\varepsilon/2}(t - \varepsilon/2)\,dt$. It is also infinitely differentiable, non-decreasing and it holds that $\mu_\varepsilon(x) = 0 \Leftrightarrow x \leqslant 0$ and $\mu_\varepsilon(x) = 1 \Leftrightarrow x \geqslant \varepsilon$.

For the given $a, b \in \mathbb{R}$ such that $a < b$ and $b - a > 2\varepsilon$ let us define the function $\eta_{a,b,\varepsilon} : \mathbb{R} \longrightarrow \mathbb{R}$ in the following way:

$$\eta_{a,b,\varepsilon}(x) = \{\begin{cases} \mu_\varepsilon(x - a), & x < (a+b)/2, \\ \mu_\varepsilon(b - x), & x \geqslant (a+b)/2. \end{cases} \tag{8}$$

This is an infinitely differentiable function equal to zero outside the interval (a, b), equal to one in the segment $[a + \varepsilon, b - \varepsilon]$, increasing in the segment $[a, a + \varepsilon]$ and decreasing in the segment $[b - \varepsilon, b]$.

Lemma 4. Let $a, b \in \mathbb{R}$ such that $a < b$ and $f, g : (a, b) \longrightarrow \mathbb{R}$ functions such that f is continuous and bounded and g s integrable without changing the sign. Then there exists $c \in (a, b)$ such that the following holds:

$$\int_a^b f(x)g(x)\,dx = f(c)\int_a^b g(x)\,dx. \tag{9}$$

Proof. Since g does not change the sign, $\int_a^b g(x)\,dx = 0$ is possible only when $g \equiv 0$ almost everywhere and in that case the claim holds true for each $c \in (a, b)$.

Let us assume, therefore, that $\int_a^b g(x)\,dx \neq 0$. In addition, if there is a constant v such that $\mu(\{x \in (a, b) | g(x) > 0, f(x) \neq v\}) = 0$ holds, then the claim holds for each c ∈(a,b) such that g(c)>0 and f(c)=v holds.

Without loss of generality, we can assume that there is no such constant v.

For

$$m = \inf_{x\in(a,b)} f(x), \quad M = \sup_{x\in(a,b)} f(x) \tag{10}$$

we have

$$\begin{aligned} m\int_a^b g(x)\,dx = \int_a^b m\,g(x)\,dx < \int_a^b f(x)g(x)\,dx \\ < \int_a^b M\,g(x)\,dx = M\int_a^b g(x)\,dx, \end{aligned} \tag{11}$$

that is

$$m < \frac{\int_a^b f(x)g(x)\,dx}{\int_a^b g(x)\,dx} < M. \tag{12}$$

Due to the continuity of the f function, there exists a $c \in (a, b)$ for which

$$f(c) = \frac{\int_a^b f(x)g(x)\,dx}{\int_a^b g(x)\,dx}, \tag{13}$$

holds and thus completes the proof of the lemma.

Lemma 5. Let $a, b, c, d \in \mathbb{R}$ be such that $a < b$, $c < d$ and $f : D \longrightarrow \mathbb{R}$ continuous function where $D = [a, b] \times [c, d]$. Then we have

$$\begin{aligned} \lim_{\varepsilon\to 0+} \iint_D f(x,y)\eta_{a,b,\varepsilon}(x)\eta'_{c,d,\varepsilon}(y)\,dx\,dy \\ = \int_a^b f(x,c)\,dx - \int_a^b f(x,d)\,dx, \end{aligned} \tag{14}$$

$$\begin{aligned} \lim_{\varepsilon\to 0+} \iint_D f(x,y)\eta'_{a,b,\varepsilon}(x)\eta_{c,d,\varepsilon}(y)\,dx\,dy \\ = \int_c^d f(a,y)\,dy - \int_c^d f(b,y)\,dy. \end{aligned} \tag{15}$$

Proof. For the given $\varepsilon > 0$, define the r_ε function as

$$r_\varepsilon(x) = \int_c^d f(x,y)\eta'_{c,d,\varepsilon}(y)\,dy - (f(x,c) - f(x,d)). \tag{16}$$

From Cantor's theorem on uniform continuity, it follows that the function f in uniformly continues and therefore the r_ε function is continuous. According to the mean value theorem, it holds that

$$\begin{aligned} \int_c^d f(x,y)\eta'_{c,d,\varepsilon}(y)\,dy &= \int_c^{c+\varepsilon} f(x,y)\omega_{\varepsilon/2}(y - c + \varepsilon/2)\,dy \\ &- int_{d-\varepsilon}^d f(x,y)\omega_{\varepsilon/2}(d - y - \varepsilon/2)\,dy \\ &= f(x,c')\int_c^{c+\varepsilon} \omega_{\varepsilon/2}(y - c + \varepsilon/2)\,dy \\ &- f(x,d')\int_{d-\varepsilon}^d \omega_{\varepsilon/2}(d - y - \varepsilon/2)\,dy \\ &= f(x,c') - f(x,d') \end{aligned} \tag{17}$$

for some $c' \in (c, c + \varepsilon)$ and $d' \in (d - \varepsilon, d)$. From there as well as from Cantor's theorem on uniform continuity, it follows that r_ε uniformly tends to zero when ε tends to zero. According to Fubini's theorem, the following holds

$$\begin{aligned} &\iint_D f(x,y)\eta_{a,b,\varepsilon}(x)\eta'_{c,d,\varepsilon}(y)\,dx\,dy \\ &= \int_a^b \int_c^d f(x,y)\eta_{a,b,\varepsilon}(x)\eta'_{c,d,\varepsilon}(y)\,dy\,dx \\ &= \int_a^b \eta_{a,b,\varepsilon}(x)\int_c^d f(x,y)\eta'_{c,d,\varepsilon}(y)\,dy\,dx \\ &= \int_a^b \eta_{a,b,\varepsilon}(x)(r_\varepsilon(x) + f(x,c) - f(x,d))\,dx \\ &= \int_a^{a+\varepsilon} (\eta_{a,b,\varepsilon}(x) - 1)(r_\varepsilon(x) + f(x,c) - f(x,d))\,dx \\ &+ \int_{b-\varepsilon}^b (\eta_{a,b,\varepsilon}(x) - 1)(r_\varepsilon(x) + f(x,c) - f(x,d))\,dx \\ &+ \int_a^b r_\varepsilon(x)\,dx + \int_a^b f(x,c)\,dx - \int_a^b f(x,d). \end{aligned} \tag{18}$$

When ε tends to zero, the first two addends tend to zero because the subintegral function is bounded as continuous on a compact set, while the third addend tends to zero on the basis of the

uniform convergence of the r_ε function to zero. From there, the first part of the claim follows while the second part can be proven analogously.

Let us further identify the complex plane with $\mathbb{R}^2$. Let Ω denote a simply connected region in the complex plane. Let $f : \Omega \longrightarrow \mathbb{C}$ which has partial derivatives f_x and f_y. The partial derivatives with respect to z and $\bar{z}$ are defined as

$$f_z = \frac{f_x - if_y}{2}, \quad f_{\bar{z}} = \frac{f_x + if_y}{2}. \tag{19}$$

Let p and q are now continuous functions which map Ω into $\mathbb{C}$ let γ denote a rectifiable curve in Ω. By the integral

$$\int_\gamma p\,dz + q\,d\bar{z} \tag{20}$$

we mean the integral

$$\int_\gamma (p+q)\,dx + i(p-q)\,dy. \tag{21}$$

NUMERICAL RESULTS

Theorem 2. The following conditions are equivalent:

A *Integral* (20) *is equal to zero with respect to each rectifiable loop γ in Ω.*

B *Integral* (20) *is equal to zero with respect to each rectangle loop γ in Ω.*

C *There exists a function $F : \Omega \longrightarrow \mathbb{C}$ which has partial derivatives and it is such that $F_z = p$ and $F_{\bar{z}} = q$.*

Proof. Since each rectangle loop is rectifiable, B follows from A. Let us derive A from C. Let us derive 1 from 3.

$$\begin{aligned} \oint_\gamma p\,dz + q\,d\bar{z} &= \oint_\gamma (p+q)\,dx + i(p-q)\,dy \\ &= \oint_\gamma (F_z + F_{\bar{z}})\,dx + i(F_z - F_{\bar{z}})\,dy \\ &= \oint_\gamma F_x\,dx + F_y\,dy = 0. \end{aligned} \tag{22}$$

Suppose that B holds and let us derive C. By a special path determined by the vertices

$$(x_0, y_0), \ldots, (x_n, y_n) \tag{23}$$

in the denotation $s[x_0, y_0; \ldots; x_n, y_n]$ we mean a zig-zag line determined by the vertices (23) so that the whole line is in Ω, that it is parameterized by a parameter from the segment $[0, 1]$, that it is linear part by part, and that, for each $k < n$ it holds $x_k = x_{k+1}$ or $y_k = y_{k+1}$. By the value along the rectifiable path γ in Ω in the denotation $V(\gamma)$ we mean value (20).

Let γ and δ be special paths such that $\gamma(0) = \delta(0)$ and $\gamma(1) = \delta(1)$. Let us prove that the following holds:

$$\int_\gamma p\,dz + q\,d\bar{z} = \int_\delta p\,dz + q\,d\bar{z}. \tag{24}$$

Let us prove it first in the case when the paths γ and δ are in the $I \times J$ set for some non-empty open intervals I and J of a real line such that $I \times J \subseteq \Omega$. Based on assumption B, for any $x_0, x_1, x_2 \in I$ and $y_0, y_1, y_2 \in J$

$$V(s[x_0, y_0; x_1, y_0; x_2, y_0]) = V(s[x_0, y_0; x_2, y_0]), \tag{25}$$

$$V(s[x_0, y_0; x_1, y_0; x_1, y_1]) = V(s[x_0, y_0; x_0, y_1; x_1, y_1]), \tag{26}$$

hold as well as

$$\begin{aligned} &V(s[x_0, y_0; x_1, y_0; x_1, y_1; x_2, y_1]) \\ &= V(s[x_0, y_0; x_1, y_0; x_2, y_0; x_2, y_1]) \\ &\quad = V(s[x_0, y_0; x_2, y_0; x_2, y_1]). \end{aligned} \tag{27}$$

Let $x_0, \ldots, x_n \in I$ and $y_0, \ldots, y_n \in J$ for $n \geqslant 2$. If there exists $i \in \{1, \ldots, n-1\}$ holds that $x_{i-1} = x_i = x_{i+1}$ or $y_{i-1} = y_i = y_{i+1}$, then there exist $x'_0, \ldots, x'_{n-1} \in I$ and $y'_0, \ldots, y'_{n-1} \in J$ such that we obtain

$$\begin{aligned} V(s[x_0, y_0; \ldots; x_n, y_n]) = V(s[x'_0, y'_0; \ldots; x'_{n-1}, y'_{n-1}]), \\ (x_0, y_0) = (x'_0, y'_0), \\ (x_n, y_n) = (x'_{n-1}, y'_{n-1}). \end{aligned} \tag{28}$$

The same also holds in the case when such i does not exist but when $n \geqslant 3$. Hence, for any $x_0, \ldots, x_n \in I$ and $y_0, \ldots, y_n \in J$ it holds that

$$\begin{aligned} V(s[x_0, y_0; \ldots; x_n, y_n]) &= V(s[x_0, y_0; x_n, y_0; x_n, y_n]) \\ &= V(s[x_0, y_0; x_1, y_n; x_n, y_n]). \end{aligned} \tag{29}$$

This means that $V(\mu)$ for the special path μ in $I \times J$ depends only on the initial and the final point of the path μ, which thus proves the claim in this case. Let us further deal with a general case.

Since Ω is a simply connected region, we can choose continuous mapping $H : [0, 1]^2 \longrightarrow \Omega$ such that for every $t \in [0, 1]$ it holds that $H(0, t) = \gamma(t)$ and $H(1, t) = \delta(t)$, and also that for every $x \in [0, 1]$ it holds that $H(x, 0) = \gamma(0) = \delta(0)$ and $H(x, 1) = \gamma(1) = \delta(1)$.

The set $H[[0, 1]^2]$ is a compact subset of the open set Ω, so there exists some $\varepsilon > 0$ such that for every $x, t \in [0, 1]$ it holds that $B(H(x, t), \varepsilon) \subseteq \Omega$.

According to Cantor's theorem on uniform continuity, there exists $n \in \mathbb{N}$ such that it holds

$$(\forall x_1, t_1, x_2, t_2 \in [0, 1])(|x_2 - x_1| + |t_2 - t_1| < 1/n \Rightarrow$$

$$d(H(x_1, t_1), H(x_2, t_2)) < \varepsilon).$$

For $i, j \in \{0, \ldots, n\}$ let us define X_i^j and Y_i^j as

$$(X_i^j, Y_i^j) = H(i/n, j/n). \tag{30}$$

Let $i_1, i_2, j_1, j_2 \in \{0, \ldots, n\}$ be such that it holds $|i_1 - i_2|, |j_1 - j_2| \leqslant 1$. Then

$$d((X_{i_1}^{j_1}, Y_{i_1}^{j_1}), (X_{i_2}^{j_2}, Y_{i_2}^{j_2})) \leqslant \varepsilon/5. \tag{31}$$

Let us also, for every $i, j \in \{0, \ldots, n\}$ define a path

$$\pi_i^j = s[x_0, y_0; \ldots; x_{2j-1}, y_{2j-1}], \tag{32}$$

where

$$(x_0, y_0) = (X_i^0, Y_i^0) = H(i/n, 0) = \gamma(0) = \delta(0), \tag{33}$$

$$(x_{2j-1}, y_{2j-1}) = (X_i^j, Y_i^j) = H(i/n, 1) = \gamma(1) = \delta(1),$$

$$x_{2k-1} = X_i^{k-1}, \quad x_{2k} = X_i^k, \quad y_{2k-1} = y_{2k} = Y_i^k, \quad \text{for } 1 \leqslant k < n.$$

For $i, k < n$ let us define the special path μ_i^k as

$$\mu_i^k = s[X_i^k, Y_i^k; X_i^k, Y_i^{k+1}; X_i^{k+1}, Y_i^{k+1}; X_i^{k+1}, Y_i^{k+1}; X_{i+1}^{k+1}, Y_{i+1}^{k+1}; X_{i+1}^k, Y_{i+1}^{k+1}; X_{i+1}^k, Y_{i+1}^k; X_{i+1}^k, Y_i^k; X_i^k, Y_i^k]. \tag{34}$$

All points of the path μ_i^k are at a mutual distance smaller than $\varepsilon/4$, so the path μ_i^k lies in $B((X_i^k, Y_i^k), \varepsilon/4)$, so there are intervals I and J of real line, which are of the width $\varepsilon/2$ and such that it holds $B((X_i^k, Y_i^k), \varepsilon/4) \subseteq I \times J \subseteq B((X_i^k, Y_i^k), \varepsilon)$. It thus follows that the path μ is in $I \times J$ and that $I \times J \subseteq \Omega$, resulting in $V(\mu_i^k) = 0$. On the basis of this, it is proven by induction that for all $i, k < n$ the following holds:

$$V(\pi_{i+1}^k) - V(\pi_i^k) = V(s[X_i^k, Y_i^k; X_{i+1}^k, Y_i^k; X_{i+1}^k, Y_i^{k+1}]). \tag{35}$$

In particular, for $k = n$ it holds that $V(\pi_i^n) = V(\pi_{i+1}^n)$, from where it follows that $V(\pi_0^n) = V(\pi_n^n)$. For any $k < n$ the restrictions of the paths π_0^n and γ on the segment $[k/n, (k+1)/n]$ have a common beginning (X_0^k, Y_0^k) and a common end (X_0^{k+1}, Y_0^{k+1}) and they are within the disc $B((X_0^k, Y_0^k), \varepsilon/4)$, so it is similarly proven as before that the integrals of $p\,dz + q\,d\bar{z}$ are equal by themselves, which therefore proves that both $V(\gamma) = V(\pi_0^n)$ i $V(\delta) = V(\pi_n^n)$.

Let us chose arbitrary(a, b) $\in \Omega$. For each $(u, v) \in \Omega$, let us define $F(u, v)$ as follows. Let γ is arbitrary special path such that $\gamma(0) = (a, b)$ and $\gamma(1) = (u, v)$ hold. Let

$$F(u, v) = \int_\gamma (p + q)\,dx + i\,(p - q)\,dy.$$

This definition is correct because of independence of the value on the choice of γ .Then $F_x = p + q$ and $F_y = i\ (p - q)$ hold and therefore $F_z = p$ and $F_{\bar{z}} = q$ hold.

Theorem 3. The following conditions are equivalent:

A *For any infinitely differentiable function $\varphi : \Omega \longrightarrow \mathbb{C}$ with compact support, it holds that*

$$\iint_\Omega p(x, y)\varphi_{\bar{z}}\,dx\,dy = \iint_\Omega q(x, y)\varphi_z\,dx\,dy.$$

B *For any closed rectangular domain $D \subseteq \Omega$ and any infinitely differentiable function $\varphi : \Omega \longrightarrow \mathbb{C}$ with support D it holds that*

$$\iint_D p(x, y)\varphi_{\bar{z}}\,dx\,dy = \iint_D q(x, y)\varphi_z\,dx\,dy.$$

C *There exists a function $F : \Omega \longrightarrow \mathbb{C}$ with continuous partial derivatives such that $F_z = p$ and $F_{\bar{z}} = q$ hold.*

Proof. It is clear that B follows from A. Suppose B and let us prove C. Let $D = [a, b] \times [c, d]$ for some $a, b, c, d \in \mathbb{R}$ such that $a < b$ and $c < d$. For $\varepsilon > 0$ such that $\varepsilon < (b-a)/2$, $(d-c)/2$ let us define h_ε, k_ε and φ_ε as

$$h_\varepsilon = \eta_{a,b,\varepsilon}, \quad k_\varepsilon = \eta_{c,d,\varepsilon}, \tag{36}$$

$$\varphi_\varepsilon : \mathbb{R}^2 \longrightarrow \mathbb{R}, \quad \varphi_\varepsilon(x, y) = h_\varepsilon(x)k_\varepsilon(y). \tag{37}$$

With the truncated forms of $p = p(x, y)$, $\varphi_\varepsilon = \varphi_\varepsilon(x, y)$, $h = h(x)$ and $k = k(y)$, it follows from B that

$$\iint_D p\,(\partial_x\varphi_\varepsilon + i\partial_y\varphi_\varepsilon)\,dx\,dy = \iint_D q\,(\partial_x\varphi_\varepsilon - i\partial_y\varphi_\varepsilon)\,dx\,dy, \tag{38}$$

$$\iint_D (p - q)\,\partial_x\varphi_\varepsilon\,dx\,dy + i\iint_D (p + q)\,\partial_y\varphi_\varepsilon\,dx\,dy = 0, \tag{39}$$
$$\iint_D (p + q)\,\partial_y\varphi_\varepsilon\,dx\,dy - i\iint_D (p - q)\,\partial_x\varphi_\varepsilon\,dx\,dy = 0.$$

On the basis of Lemma 5, allowing ε to tend to zero, we conclude that the following holds

$$\int_a^b (p + q)(x, c)\,dx - \int_a^b (p + q)(x, d)\,dx + i$$
$$+ \int_c^d (p - q)(a, y)\,dy - i\int_c^d (p - q)(b, y)\,dy = 0, \tag{40}$$

namely

$$\oint_{\partial D} (p + q)\,dx + i(p - q)\,dy = 0, \tag{41}$$

so on the basis of Theorem 2 it holds B. Let us suppose C and let us derive A. It should be actually proven that the following holds

$$\iint_\Omega F_z\varphi_{\bar{z}}\,dx\,dy = \iint_\Omega F_{\bar{z}}\varphi_z\,dx\,dy, \tag{42}$$

i.e.

$$\iint_\Omega (F_x - iF_y)(\varphi_x + i\varphi_y)\,dx\,dy \tag{43}$$
$$= \iint_\Omega (F_x + iF_y)(\varphi_x - i\varphi_y)\,dx\,dy,$$

which is equivalent to

$$\iint_\Omega F_x\varphi_y\,dx\,dy = \iint_\Omega F_y\varphi_x\,dx\,dy. \tag{44}$$

Let $K \subseteq \Omega$ be a compact support of the function φ. Each point of the set K can be paired with an open rectangle whose sides are parallel to the coordinate axes and whose closure lies in Ω. Such a cover has a definite subcover; therefore, without loss of generality, we can assume that K is a non-empty finite union of closed rectangles with non-empty interior and sides parallel to the coordinate axes.

Suppose that $D = [a, b] \times [c, d]$ is the smallest closed rectangle with its sides parallel to the coordinate axes, such that $K \subseteq D$. Let us pair each $x \in [a, b]$ with the set

$$D_x = \{y \in [c, d]\ :\ (x, y) \in K\}. \tag{45}$$

For each x, the set D_x is a finite union of disjoint closed intervals. On the endpoints of each of these intervals, the function φ is annuled together with its partial derivatives. Hence, if $[u, v]$ is some of these intervals, then it holds that

$$\begin{aligned}\int_u^v F_y(x,y)\varphi_x(x,y)\,dy &= F(x,v)\varphi_x(x,v) - F(x,u)\varphi_x(x,u) \\ &- \int_u^v F(x,y)\varphi_{xy}(x,y)\,dy \\ &= -\int_u^v F(x,y)\varphi_{xy}(x,y)\,dy.\end{aligned} \tag{46}$$

By adding the integrals as a function of all disjoint closed intervals which give the set D_x in the union, we conclude that the following holds

$$\int_{D_x} F_y(x,y)\varphi_x(x,y)\,dy = -\int_{D_x} F(x,y)\varphi_{xy}(x,y)\,dx\,dy. \tag{47}$$

According to Fubini's theorem, we have

$$\begin{aligned}\iint_K F_y(x,y)\varphi_x(x,y)\,dx\,dy &= \int_a^b \int_{D_x} F_y(x,y)\varphi_x(x,y)\,dx\,dy \\ &= -\int_a^b \int_{D_x} F(x,y)\varphi_{xy}(x,y)\,dx\,dy \\ &= -\iint_K F(x,y)\varphi_{xy}(x,y)\,dx\,dy.\end{aligned} \tag{48}$$

Since K is the support of the function φ, it holds that

$$\begin{aligned}&\iint_\Omega F_y\varphi_x\,dx\,dy = \iint_K F_y\varphi_x\,dx\,dy = \\ -\quad &\iint_K F(x,y)\varphi_{xy}(x,y)\,dx\,dy = -\iint_\Omega F(x,y)\varphi_{xy}(x,y)\,dx\,dy.\end{aligned} \tag{49}$$

The formula

$$\iint_\Omega F_x\varphi_y\,dx\,dy = -\iint_\Omega F(x,y)\varphi_{xy}(x,y)\,dx\,dy, \tag{50}$$

is similarly proven thus finally leading to (44).

APPENDIX

Recall that this paper is related to a paper by authors Arsenović, M. and Mateljević, M. titled "On Ahlfors-Beurling Operator" published in Journal of Mathematical Sciences, 2021 (referenced below Arsenović, M., Mateljević, M. On Ahlfors–Beurling Operator. J Math Sci 259, 1–9 (2021). https://doi.org/10.1007/s10958-021-05596-9)

In the above mentioned paper authors Miodrag Mateljević and Miloš Arsenović investigate regularity properties of solutions of Beltrami equation expressed in terms of moduli of continuity. Authors Miodrag Mateljević and Miloš Arsenović prove that a class of Calderon-Zygmund operators, including Ahlfors-Beurling operator, preserves certain type of modulus of continuity of compactly supported functions. They have also proved a purely topological result which easily gives injectivity of normal solutions of Beltrami equation.

Theorem 1 and Theorem 2 from the above mentioned paper are given below. In order to make it easier for readers to understand the problems that the authors Miodrag Mateljević and Miloš Arsenović deal with in the mentioned paper, a complete proof of Theorem 1 is given.

For the convenience of the readers, some definitions, terms and considerations will be mentioned (in the same way as presented in the mentioned paper).

Authors choose a majorant ω i.e. a continuous increasing and concave function, $\omega(t)$, $t \geqslant 0$ such that $\omega(0) = 0$ and $\omega(\lambda t) \leqslant C_\lambda \omega(t)$, $\lambda > 1$.

Authors impose the following two conditions on majorant ω:

$$\int_0^1 \frac{\omega(t)}{t}\,dt \leqslant A_1\omega(\delta), \quad 0 < \delta < 1. \tag{1}$$

$$\int_0^1 \frac{\omega(t)}{t}\,dt \leqslant A_2\frac{\omega(\delta)}{\delta}, \quad 0 < \delta < 1. \tag{2}$$

The operator T is defined by the following formula:

$$Tf(x) = \lim_{\varepsilon\to 0}\int_{\mathbb{R}^n} K_\varepsilon(y) f(x-y)\,dy,$$

where K_ε denotes a truncated kernel

$$K_\varepsilon(x) = \begin{cases} K(x), & |x| \geqslant \varepsilon, \\ 0, & |x| < \varepsilon. \end{cases}$$

In the same paper it is proved:

$$Tf(x) = \int K(y)[f(x-y) - f(x)]\,dy, \quad x \in \mathbb{R}^n \tag{3}$$

Theorem 1. Assume a majorant ω satisfies conditions (1) and (2). Then for every $R > 0$ there is a constant $C = C(R, n, \Omega, \omega)$ such that

$$\|Tf\|_\omega \leqslant C\|f\|_\omega, \quad f \in \wedge_\omega^R. \tag{4}$$

We note the following well known estimate for the kernel K:

$$|K(x+h) - K(x)| \leqslant C(\Omega)\frac{|h|}{|x|^{n+1}}, \quad x \neq 0, h \leqslant |x|/3. \tag{5}$$

Let us choose $f \in \Lambda_\omega^R$ and $x, x+h \in \mathbb{R}^n$, where $|h| \leqslant 1$. From (3) we obtain

$$Tf(x) = \left(\int_{|y|\leqslant 3|h|} + \int_{3|h|\leqslant y\leqslant |x|+R}\right) K(y)[f(x-y) - f(x)]\,dy = I_1 + I_2. \tag{6}$$

Analogously to the argument leading to (11) we estimate I_1:

$$\|I_1\| \leqslant \|\Omega\|_\infty \|f\|_\omega |S^{n-1}| \int_0^{3|h|} \frac{\omega(t)}{t}\,dt \leqslant C(n,\Omega,\omega)\|f\|_\omega\omega(|h|). \tag{7}$$

where we used condition (1). Replacing x with $x + h$ in (6) we obtain

$$Tf(x) = \left(\int_{|y|\leqslant 3|h|} + \int_{3|h|\leqslant y\leqslant |x|+R}\right) K(y)[f(x+h-y) - f(x+h)]\,dy = J_1 + J_2, \tag{8}$$

where $|J_1| \leqslant C(n,\Omega,\omega)\|f\|_\omega\omega(|h|)$ and

$$\begin{aligned} J_2 &= \int_{3|h|\leqslant|y|\leqslant|x+h|+R} K(y)[f(x+h-y)-f(x+h)]\,dy \\ &= \int_{3|h|\leqslant|y|\leqslant|x+h|+R} K(y)[f(x+h-y)-f(x)]\,dy \qquad (9) \\ &= \int_{3|h|\leqslant|z+h|\leqslant|x+h|+R} K(z+h)[f(x-z)-f(x)]\,dz \\ &= \int_{3|h|\leqslant|z|\leqslant|x|+R} K(z+h)[f(x-z)-f(x)]\,dz + E = \tilde{J}_2 + E. \end{aligned}$$

Note that cancellation property enabled replacement of $f(x+h)$ with $f(x)$. Now we estimate the error term E, which results from a change of domain of integration from one spherical ring $A(-h;3|h|;|x+h|+R)$ to another one $A(0;3|h|;|x|+R)$. Regarding the change of inner limits, the size of $K(z+h)$ is estimated by $C(n)\|\Omega\|_\infty|h|^{-n}$, the measure of the symmetric difference of $B(0;3|h|)$ and $B(-h;3|h|)$ is estimated by $C(n)|h|^n$ and the size of $f(x-z)-f(x)$ is estimated by $C(\omega)\|f\|_\omega\omega(|h|)$. Hence the error due to the change of inner limits is estimated by $C(n,\Omega,\omega)\|\Omega\|_\infty\omega(|h|)$.

Regarding the change of outer limits, the measure of the symmetric difference of domains of integration is estimated by $C(n)|h|(|x|+R)^{n-1}$, the size of $K(z+h)$ by $\|\Omega\|_\infty(|x|+R)^{-n}$ and the size of $f(x-z)-f(x)$ by $2\|f\|_\infty$, hence the contribution to the error term is bounded by $C\|\Omega\|_\infty\|f\|_\infty|h|$, where C is a constant depending only on n. Since $\|f\|_\infty \leqslant C(\omega,R)\|f\|_\omega$ and $\delta \leqslant C_\omega(\delta)$ for $0 \leqslant \delta \leqslant 1$ we obtain

$$|E| \leqslant C(R,n,\Omega,\omega)\|f\|_\omega\omega(|h|). \qquad (10)$$

Combining (6), (7), (8), (9) and (10) we obtain

$$\begin{aligned} |Tf(x+h)-Tf(x)| &= |J_1+\tilde{J}_2+E-I_1-I_2| \\ &\leqslant |\tilde{J}_2-I_2|+|E|+|I_1|+|J_1| = E_1+E_2 \end{aligned}$$

where

$$E2 = |E|+|I_1|+|J_1| \leqslant C(R,n,\Omega,\omega)\|f\|_\omega\omega(|h|)$$

and

$$E_1 = \left|\int_{3|h|\leqslant|z|\leqslant|x|+R}[K(z+h)-K(z)][f(x-z)-f(x)]\,dz\right|.$$

Since f is supported in $B(0;R)$ we can assume $\omega(t)$s is constant for $t \geqslant 2R$, in particular $\omega(t) \leqslant \omega(2R)$. We use (5) and (2) to estimate E_1:

$$\begin{aligned} E_1 &\leqslant C(\Omega)\int_{3|h|\leqslant|z|\leqslant|x|+R}\frac{|h|}{|z|^{n+1}}|f(x-z)-f(x)|\,dz \\ &\leqslant C(\Omega)|h|\|S^{n-1}\|\|f\|_\omega\int_{3|h|}^{|x|+R}\frac{\omega(t)}{t^2}\,dt \\ &= |h|C(n,\Omega)\|f\|_\omega\left(\int_{3|h|}^{1}+\int_1^\infty\right)\frac{\omega(t)}{t^2}\,dt \\ &\leqslant C_n\|f\|_\omega(A_2\omega(|h|)+\omega(2R)|h|) \\ &\quad C(R,n,\Omega,\omega)\|f\|_\omega\omega(|h|). \end{aligned}$$

Note that this was the only estimate in the proof that relied on (2). This gives desired estimate for $|h| \leqslant 1$, the estimate for $|h| > 1$ follows easily from the vanishing of Tf at infinity. In fact, since the support of f is compact we have the following asymptotic: $Tf(x) = O(|x|^{-n}))$ as $x \to +\infty$; we leave details to the reader.

Theorem 2. Let f be a quasiconformal mapping between bounded planar domains D and G with $C^{1,\alpha}$ boundaries, where $0 < \alpha < 1$. Then the following three conditions are equivalent.

(A) $f \in C^{1,\alpha}(\overline{D})$ and $f^{-1} \in C^{1,\alpha}(\overline{G})$.

(B) The complex dilatation μ_f is α Hölder continuous on D.

(C) The complex dilatation $\mu_{f^{-1}}$ is α Hölder continuous on G.

REFERENCES

Ahlfors, L. 2006, Lectures on Quasiconformal Mappings, University Lecture Series, vol.38, 2nd edn. American Mathematical Society, Providence

Arsenović, M. & Mateljević, M. 2021, On Ahlfors-Beurling Operator, Journal of Mathematical Sciences, 259, pp. 1-9. https://doi.org/10.1007/s10958-021-05596-9

Arsenović, M., Mateljević, M., & Ahlfors, O. 2012, Teorija mere, funkcionalna analiza, teorija operatora (Zavod za udžbenike, Beograd)

Carleson, L. & Jones, P. 1992, On coefficient problems for univalent functions and conformal dimension. Duke Mathematical Journal. 66. DOI: 10.1215/S0012-7094-92-06605-1

Duren, P. 2004, Harmonic Mapping in the Plane, Cambridge University Press, Cambridge

Mateljević, M. 2012, Topic in Conformal, Quasiconformal and Harmonic Maps (Zavod za udžbenike, Beograd)

Mateljević, M. 2013a, Kompleksna analiza 1 (Zavod za udžbenike, Beograd)

Mateljević, M. 2013b, Kompleksna analiza 2 (Zavod za udžbenike, Beograd)

Bulletin of Natural Sciences Research
Vol.12, No.2, 2022. pp. 31-35.

DOI: https://doi.org/10.5937/bnsr12-40124
Original Scientific Paper

NOMA COOPERATIVE RELAYING SYSTEMS OVER RICIAN-SHADOWED FADING CHANNELS

STEFAN R. PANIĆ[1,⋆], SERGEI KHOTNENOK[2]

[1]Faculty of Sciences and Mathematics, University of Priština in Kosovska Mitrovica, Serbia
[2]Tomsk State University of Control Systems and Radioelectronics, Tomsk, Russia

ABSTRACT

Non-orthogonal multiple Access (NOMA) is an efficient 5G technology that enables network spectral efficiency increase and network access latency. In order to additionally improve the reliability of transmission and increase the achievable rate of NOMA system, combined utilization of NOMA and cooperative relay transmission (CRS) could appear as effective remedy. In this work, we will carry out performance analysis of NOMA based CRS over Rician-Shadowed fading channels. The closed-form expression for the exact average achievable rate is presented in the form of Meijer G functions infinite-series. Numerical results are presented in order to manifest the credibility of the presented method.

Keywords: Average achievable rate, CRS, Rician-Shadowed fading, NOMA.

INTRODUCTION

Non-orthogonal multiple access (NOMA) has emerged as an effective technology for increasing spectral efficiency of 5G downlink networks and while increasing networks access latency (Wei et al., 2017). Opposite to regular orthogonal multiple access (OMA) the main concept of NOMA is to explore the power domain in order to provide multiple access to users with distinct power levels, while using at the reception the principle of successive interference cancellation (SIC) after decoding the highest quality signal, in order to decode the remaining signals. For the purpose of further improvement of the reliability of NOMA transmission and increase the achievable NOMA rate, combined utilization of NOMA and cooperative relay transmission (CRS) could be used. CRS NOMA system realizations and their performances have been often discussed in literature recently: Jiao et al. (2017); Duan et al. (2018); Liang et al. (2016); Men & Ge (2016); Kim & Lee (2015); Ding et al. (2015); Wan et al. (2018); Jha & Kumar (2018); Jha et al. (2018); Panic & Jayakody (2019).

In 5G signal propagation theory most observed is case when transmitted signal with the strong LOS (line-of-sight) component propagates together along different non-LOS paths, so various LOS shadow fading effects occur due to total or partial blockage of the LOS by corresponding obstacles that appear or move on a direction between the transmitter and receiver. As the result of this blockage, the amplitude of the LOS component behaves a random process, so signal propagation can be accurately modeled with shadowed Rician fading model Simon & Alouini (2005). This model serves as good representation for 4 different shadowing scenarios: light shadowing scenario, heavy shadowing scenario, overall shadowing scenario and average shadowing scenario. Also this model could correctly represent random fluctuations at the reception caused by fading and shadowing that occur separately Simon & Alouini (2005).

In Kim & Lee (2015) performance analysis of the CRS NOMA over both Rayleigh fading channels and Hoyt fading channels were carried out, but only asymptotic expression are provided for the achievable rate criterion. In Jiao et al. (2017) performance analysis of CRS NOMA over Rician fading channels were carried out, but only expressions for approximating the achievable rate based on the Gauss-Chebyshev method Hildebrand (1987) have been introduced. Identical approximation method has been used in Jha & Kumar (2018); Jha et al. (2018) to deliver achievable rate of an Opportunistic CRS NOMA over Rician fading channels for the case of available CSI (Channel State Information). In Panic & Jayakody (2019) closed form expressions have been provided for the achievable average rate of the NOMA based CRS over Hoyt fading channels. However, to the best of the authors knowledge, there is no work reported in literature, where closed form expressions have been provided for the achievable average rate of NOMA based CRS over Rician-Shadowed fading channels.

In this work we will carry out the performance analysis of NOMA based CRS over Rician-Shadowed fading channels and deliver rapidly converging infinite series expression for the average achievable rate in the form of of Meijer G functions. Numerical results will be delivered and analyzed in the function of Rician-Shadowed fading severity parameters.

SYSTEM MODEL

We are observing cooperative relaying system composed of a source node (S), a relay node (R) with decode-and-forward (DF) performed in in half-duplex (HD) mode, and a destination node (D), where is assumed that all the links, i.e., S-D, S-R, and R-D are ready for transmission. The Rician Shadowed modeled fading

⋆ Corresponding author: stefan.panic@pr.ac.rs

channel coefficients of S-D, S-R, and R-D links are denoted with h_{SD}, h_{SR}, and h_{RD}, while Ω_{SD}, Ω_{SR}, and Ω_{RD}, denote corresponding average powers, respectively. As it is assumed that the path loss of the S-D link is higher the path loss of the S-R link, we are observing the case when stands $\Omega_{SD} < \Omega_{SR}$. The system model of NOMA-based CRS is showed in Fig. 1. The advantage of such architecture comes from the ability that system is capable of receiving distinct signals in distinct time slots at the destination, so it can outperform the traditional CRS system throughput performances, as illustrated in Kim & Lee (2015). Namely, NOMA-based CRS transmits two signals in two slots, so it easily outperforms traditional CRS concept that only transmits one signal during time.

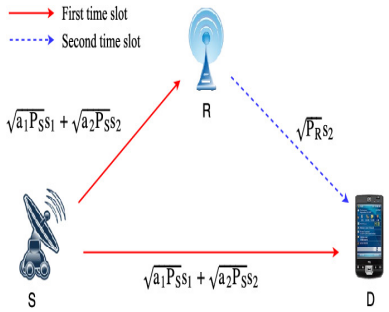

Figure 1. NOMA-based CRS scheme.

The source transmits in the first time slot the superposition of two distinct symbols: s_1 and s_2, to both R and D. Allow us represent i-th transmittion symbol with s_i, whose normalized power is $E(|s_i|^2) = 1$, while let P_t denote the total transmit power, a_i the power allocation coefficient, where stands $a_1 + a_2 = 1$, and $a_1 > a_2$, due to $\Omega_{SD} < \Omega_{SR}$. At the destination only symbol s_1 is decoded, while symbol s_2 is observed as noise, so R acquires symbol s_2 using SIC. In the second time slot, R only transmits to D the decoded symbol s_2 with total power P_t, assuming that R have perfectly decoded symbol s_2 at first time slot. Therefore, the received signals r_{sr} and r_{sd} in the first time slot, and the received signal in the second time slot, r_{rd}, can be represented as:

$$\begin{aligned} t &= \sqrt{a_1 P_t} s_1 + \sqrt{a_2 P_t} s_2, \\ r_{sr} &= h_{sr} t + n_{sr}, \\ r_{sd} &= h_{sd} t + n_{sd}, \\ r_{rd} &= h_{rd} P_t s_2 + n_{rd}, \end{aligned} \tag{1}$$

where n_{SR}, n_{RD} and n_{SD} denote the additive white Gaussian noise (AWGN) of zero mean and variance σ^2. Consequently, signal-to-interference plus noise ratios (SINRs) of symbols s_1 and s_2 at the relay can be represented as:

$$\begin{aligned} \gamma_{sr}^1 &= \frac{|h_{sr}|^2 a_1 P_t}{|h_{sr}|^2 a_2 P_t + \sigma^2}, \\ \gamma_{sr}^2 &= \frac{|h_{sr}|^2 a_2 P_t}{\sigma^2}, \\ \gamma_{sd} &= \frac{|h_{sd}|^2 a_1 P_t}{|h_{sd}|^2 a_2 P_t + \sigma^2}, \\ \gamma_{rd} &= \frac{|h_{rd}|^2 P_t}{\sigma^2}. \end{aligned} \tag{2}$$

Achievable rate analysis

Here we will consider the average achievable rate of signals s_1 and s_2. Let $\lambda_{SD} = |h_{SD}|^2$, $\lambda_{SR} = |h_{SR}|^2$, $\lambda_{RD} = |h_{RD}|^2$, and $\rho = P_t/\sigma^2$, where ρ denotes the transmit SNR. Since both signals, s_1 and s_2, should be successfully decoded at both relay and the destination then corresponding rates of these two signals should be lower than the rates of both links, and therefore achievable rate can be observed as the minimum of the rates of two different links. Based on above-mentioned the achievable rates C_{s_1} and C_{s_2} of signals s_1 and s_2 could be respectively expressed as:

$$\begin{aligned} C_{s1} &= \frac{1}{2} \min\{\log_2(1+\gamma_{sd}), \log_2(1+\gamma_{sr}^1)\} \\ &= \frac{1}{2} \left(\log_2(1+\min\{\lambda_{sd}, \lambda_{sr}\}\rho) - \log_2(1+\min\{\lambda_{sd}, \lambda_{sr}\}\rho a_2)\right); \\ C_{s2} &= \frac{1}{2} \min\{\log_2(1+\gamma_{rd}), \log_2(1+\gamma_{sr}^2)\} \\ &= \frac{1}{2} \log_2(1+\min\{a_2\lambda_{sr}, \lambda_{rd}\}\rho), \end{aligned} \tag{3}$$

There arises a necessity to observe scenario when obstacles block the LOS link in between relay nodes and LOS signal fluctuations are affected by shadowing effect. Various studies have demonstrated that the Rician-Shadowed fading model provides a good match to 5G channel estimations in a various propagation cases, and spreads wide scope of fading conditions from strong LOS fading model to heavy shadowed NLOS model, and in that way Rician-Shadowed offers a possibility to characterize fading environments which are more intense than those characterized by the Rician fading model. PDF of Rician-shadowed distributed SNR can be presented as Panic et al. (2013):

$$\begin{aligned} f_{\lambda_i}(\lambda_i) &= \frac{m_i^{m_i}(1+\kappa_i)}{(\kappa_i+m_i)^{m_i}\bar{x}_i} \exp\left(-\frac{(1+\kappa_i)\lambda_i}{\bar{x}_i}\right) \\ &\times {}_1F_1\left(m_i, 1, \frac{\kappa_i(1+\kappa_i)\lambda_i}{\bar{x}_i(m_i+\kappa_i)}\right), \end{aligned} \tag{4}$$

where ${}_1F_1(x)$ represents the confluent hypergeometric function of first kind Gradshteyn & Ryzhik (2007), parameter $2b_i$ denotes the average power of scatter component, while parameter m_i expresses fading severity magnitude. Further, parameter κ_i defines the ratio of powers, $\kappa_i = \frac{\Omega_i}{2b_i}$, Ω_i stands for the average power of LOS component, while $\bar{x}_i$, $\bar{x}_i = E[X_i]$, represents average channel SNR value. Rician-Shadowed link parameter values for corresponding

shadowing mode are provided in Abdi et al. (2003) as: heavy shadowing ($m_i = m_j = 0.739$, $b_i = b_j = 0.063$, $\kappa_i = \kappa_j = 0.00711$, $\bar{x}_i = \bar{x}_j = 8.97\times10^{-4}$), average shadowing ($m_i = m_j = 10.1$, $b_i = b_j = 0.126$, $\kappa_i = \kappa_j = 4.0828$, $\bar{x}_i = \bar{x}_j = 0.835$), overall shadowing ($m_i = m_j = 5.21$, $b_i = b_j = 0.251$, $\kappa_i = \kappa_j = 0.55387$, $\bar{x}_i = \bar{x}_j = 0.278$) and light shadowing ($m_i = m_j = 19.4$, $b_i = b_j = 0.158$, $\kappa_i = \kappa_j = 2.64241$, $\bar{x}_i = \bar{x}_j = 1.29$). Following Popovic et al. (2011), we can express the cumulative distribution function (CDF) of $z = min\{\lambda_i, \lambda_j\}, (i, j) \in (SD, SR, RD)$ as:

$$\begin{aligned} &F_z(z) = 1 - P(\lambda_i > z)P(\lambda_j > z) = \\ &1 - (1 - P(\lambda_i < z))(1 - P(\lambda_j < z)) = \\ &= F_{\lambda_i}(z) + F_{\lambda_j}(z) - F_{\lambda_i}(z)F_{\lambda_j}(z) = \\ &1 - \sum_{p=0}^{\infty}\sum_{l=0}^{p} \frac{m_i\kappa_i^p(1+\kappa_i)^l\Gamma(m_i+p)z^l}{(\kappa_i+m_i)^{m_i}\bar{x}_i{}^l\Gamma(m_i)(p!)^2l!} \quad \exp\left(-\frac{(1+\kappa_i)z}{\bar{x}_i}\right) \\ &\times\sum_{q=0}^{\infty}\sum_{s=0}^{q} \frac{m_j\kappa_j^q(1+\kappa_j)^s\Gamma(m_j+q)z^s}{(\kappa_j+m_j)^{m_j}\bar{x}_j{}^l\Gamma(m_j)(q!)^2s!} \quad \exp\left(-\frac{(1+\kappa_j)z}{\bar{x}_j}\right), \end{aligned} \tag{5}$$

where $\gamma(a, x)$, denotes lower incomplete Gamma function Gradshteyn & Ryzhik (2007).

Now, in order to escape from the usage of the Gauss-Chebyshev approximation, that is heavily conditioned on the order of approximation, and in order to acquire closed form solution for achievable rate expressions over Rician-Shadowed fading channels, we must define expression for C_{s_1}:

$$C_{s1} = \frac{1}{2}\int_0^{\infty} (\log_2(1 + z_1\rho) - \log_2(1 + z_1a_2\rho))\, f_z(z)dz, \tag{6}$$

and derive closed-form expressions based on the PDF expression of $z = min\{\lambda_i, \lambda_j\}, (i, j) \in (SD, SR, RD)$, that is expressed according to (5) as:

$$f_z(z) = f_{\lambda_i}(z) + f_{\lambda_j}(z) - f_{\lambda_i}(z)F_{\lambda_i}(z) - f_{\lambda_j}(z)F_{\lambda_i}(z). \tag{7}$$

By replacing (4) and (5) in (7), and carrying out some basic mathematical manipulations, namely by presenting lower incomplete gamma function, $\gamma(a, x)$, in the form of hypergeometric function ${}_1F_1(a, b, x)$, by using (§8.351.2) from Gradshteyn & Ryzhik (2007) and capitalizing on series representation, given with (9.210/1) from Gradshteyn & Ryzhik (2007), and beyond by noticing that logarithmic function can be represented through Meijer G function by using (11) from Gradshteyn & Ryzhik (1990): $\ln(1 + x) = G_{1,2}^{2,2}\left(\begin{matrix}1,1\\0,0\end{matrix}\middle|x\right)$, and finally by using the expression, (27) from Gradshteyn & Ryzhik (1990):

$$\begin{aligned} &\int_0^{\infty} x^{-\alpha}\exp(-\omega x)\, G_{p,q}^{m,n}\left(\begin{matrix}a_p\\b_q\end{matrix}\middle|\eta x\right)dx = \\ &\omega^{\alpha-1}G_{p+1,q}^{m,n+1}\left(\begin{matrix}\alpha, a_p\\b_q\end{matrix}\middle|\frac{\eta}{\omega}\right), \end{aligned} \tag{8}$$

expressions for achievable rates can now be expressed in the form of $I_1(\rho)$ and $I_1(\rho a_2)$, through Meijer G function infinite series sums as:

$$C_{s1} = I_1(\rho) - I_1(\rho a_2), \tag{9}$$

where only 15-25 terms should be summed in both infinite sum to attain accuracy at 4^{th} significant digit. In similar manner C_{s2} can be presented through rapidly-converging Meijer G function infinite series sums, beginning from

$$C_{s2} = \frac{1}{2}\int_0^{\infty} (\log_2(1 + y\rho)\, f_y(y)dy, \tag{10}$$

by using the fact that variable y can be expressed as y=min($a_2\lambda_{sr}, \lambda_{rd}$), when acquiring its CDF and PDF.

In presented expressions for C_{s2} and $I_1(\rho)$, given with Eq.(11), factor $(a)_n$ stands for the Pochhammer symbol, defined in ((6.1.22) from Gradshteyn & Ryzhik (2007).

$$\begin{aligned} C_{s1} = {} & \tfrac{1}{2ln2}\sum_{q=0}^{\infty}\sum_{p=0}^{\infty}\sum_{l=0}^{p} \frac{m_im_j\kappa_j^q\kappa_i^p\Gamma(m_i+p)\Gamma(m_j+q)(1+\kappa_i)^l(1+\kappa_j)^{q+1}\bar{x}_i{}^{q+1}\bar{x}_j{}^l}{(\kappa_i+m_i)^{m_i}(\kappa_j+m_j)^{m_j}\Gamma(m_i)\Gamma(q)(p!)^2(q!)^2l!((1+\kappa_i)\bar{x}_j+(1+\kappa_j)\bar{x}_i)^{q+l+1}} \\ &\times\left(\rho G_{1,3}^{3,2}\left(\begin{matrix}-q-l, 1, 1\\1, 0\end{matrix}\middle|\frac{\rho\bar{x}_i\bar{x}_j}{(1+\kappa_i)\bar{x}_j+(1+\kappa_j)\bar{x}_i}\right) - a\rho G_{1,3}^{3,2}\left(\begin{matrix}-q-l, 1, 1\\1, 0\end{matrix}\middle|\frac{a\rho\bar{x}_i\bar{x}_j}{(1+\kappa_i)\bar{x}_j+(1+\kappa_j)\bar{x}_i}\right)\right) + \\ &\tfrac{1}{2ln2}\sum_{q=0}^{\infty}\sum_{p=0}^{\infty}\sum_{s=0}^{q} \frac{m_im_j\kappa_j^q\kappa_i^p\Gamma(m_i+p)\Gamma(m_j+q)(1+\kappa_i)^s(1+\kappa_j)^{p+1}\bar{x}_i{}^{p+1}\bar{x}_j{}^s}{(\kappa_i+m_i)^{m_i}(\kappa_j+m_j)^{m_j}\Gamma(m_i)\Gamma(q)(p!)^2(q!)^2s!((1+\kappa_i)\bar{x}_j+(1+\kappa_j)\bar{x}_i)^{p+s+1}} \\ &\times\left(\rho G_{1,3}^{3,2}\left(\begin{matrix}-p-s, 1, 1\\1, 0\end{matrix}\middle|\frac{\rho\bar{x}_i\bar{x}_j}{(1+\kappa_i)\bar{x}_j+(1+\kappa_j)\bar{x}_i}\right) - a\rho G_{1,3}^{3,2}\left(\begin{matrix}-p-s, 1, 1\\1, 0\end{matrix}\middle|\frac{a\rho\bar{x}_i\bar{x}_j}{(1+\kappa_i)\bar{x}_j+(1+\kappa_j)\bar{x}_i}\right)\right); \end{aligned} \tag{11}$$

$$\begin{aligned} C_{s2} = {} & \tfrac{1}{2ln2}\sum_{q=0}^{\infty}\sum_{p=0}^{\infty}\sum_{l=0}^{p} \frac{m_im_j\kappa_j^q\kappa_i^p\Gamma(m_i+p)\Gamma(m_j+q)(1+\kappa_i)^l(1+\kappa_j)^{q+1}\bar{x}_i{}^{q+1}\bar{x}_j{}^la^{q+1}}{(\kappa_i+m_i)^{m_i}(\kappa_j+m_j)^{m_j}\Gamma(m_i)\Gamma(q)(p!)^2(q!)^2l!((1+\kappa_i)\bar{x}_j+(1+\kappa_j)\bar{x}_ia)^{q+l+1}}\left(\rho G_{1,3}^{3,2}\left(\begin{matrix}-q-l, 1, 1\\1, 0\end{matrix}\middle|\frac{a\rho\bar{x}_i\bar{x}_j}{(1+\kappa_i)\bar{x}_j+(1+\kappa_j)\bar{x}_i}\right)\right) + \\ &\tfrac{1}{2ln2}\sum_{q=0}^{\infty}\sum_{p=0}^{\infty}\sum_{s=0}^{q} \frac{m_im_j\kappa_j^q\kappa_i^p\Gamma(m_i+p)\Gamma(m_j+q)(1+\kappa_i)^s(1+\kappa_j)^{p+1}\bar{x}_i{}^{p+1}\bar{x}_j{}^sa^{p+1}}{(\kappa_i+m_i)^{m_i}(\kappa_j+m_j)^{m_j}\Gamma(m_i)\Gamma(q)(p!)^2(q!)^2s!((1+\kappa_i)\bar{x}_j+(1+\kappa_j)\bar{x}_ia)^{p+s+1}}\left(\rho G_{1,3}^{3,2}\left(\begin{matrix}-p-s, 1, 1\\1, 0\end{matrix}\middle|\frac{a\rho\bar{x}_i\bar{x}_j}{(1+\kappa_i)\bar{x}_j+(1+\kappa_j)\bar{x}_i}\right)\right); \end{aligned}$$

NUMERICAL RESULTS

Rician-Shadowed fading severity over corresponding relay links can be defined through set of parameters (m_i, b_i, κ_i, $\bar{x}_i$) $i \in (RS, SD, RD)$, while as explained in Panic & Jayakody (2019) a represents the power allocation coefficient. Parameter $\bar{x}_i$, $i \in (RS, SD, RD)$, denotes the average power gains of links S-D, S-R, R-D, mostly mirroring the impact of relay node lengths. Since is assumed that the S-R and R-D distances are generally smaller than the S-D distance, then links S-R and R-D should have larger average power gains than S-D link, which corresponds

to values of $\bar{x}_{SD} < \bar{x}_{SR} \leq \bar{x}_{RD}$.

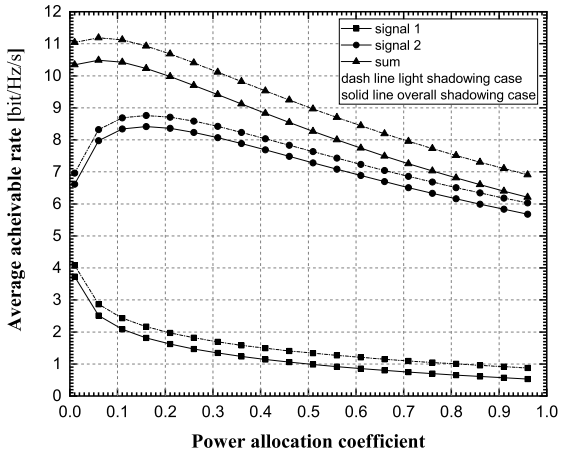

Figure 2. Achievable rates for the CRS NOMA over Rician-Shadowed fading channels.

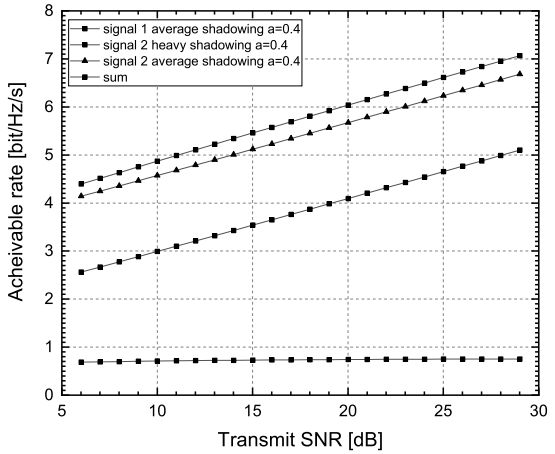

Figure 3. Achievable rates for the CRS NOMA over Rician-Shadowed fading channels.

At Fig. 2 the achievable rate performances of s_1, s_2 are presented along with the equivalent sum rate of the CRS NOMA in the function of the power allocation coefficient a. We have predefined SNR value to SNR=20 dB, $\bar{x}_{SD} = 2$, $\bar{x}_{RS} = \bar{x}_{RD} = 10$, and Rician-Shadowed channel conditions of light shadowing and overall shadowing. As expected, when a parameter increases, signal s_2 reaches more power so its achievable rate consequently increases, while simultaneously corresponding achievable rate of signal s_1 will decrease. Sum rate of two signals will first increase and then will further decrease with the growth of a parameter values. It can be seen that for smaller a values the achievable rate of signal s_2 is mostly influenced by link S-R, since $a_2\lambda_{SR} < \lambda_{RD}$. Because of SIC, signal s_2 would have no interference in S-R link, so increase in a would lead to increase the achievable rate of signal s_2, and consequently to increase in total sum rate. Afterwards, when a increases, $a\lambda_{SR}$ becomes than λ_{RD}, so the rate of link R-D will becomes the uppermost reason, which would cause that achievable rate of signal s_2 finally could not recompense for the decrease of s_1 achievable rate, so total rate would also notably decrease. We can observe from figure that there lays an optimal power allocation coefficient that can be used to maximise the sum rate.

Fig. 3 presents the achievable rates of the NOMA-based CRS against the transmit SNR, for Rician-Shadowed channel conditions of heavy shadowing and average shadowing where we set $a = 0.4$, $\bar{x}_{SD} = 2$, $\bar{x}_{RS} = 10$, and $\bar{x}_{RD} = 15$. As expected it is obvious that better results are received for average shadowing condition case.

CONCLUSION

In this work, we have carried out performance analysis of NOMA based CRS over Rician-Shadowed fading channels and presented the exact analytical expressions of the achievable rates. Expression have been provided in the form of Meijer G function infinite-series sums that rapidly converge.Numerical results have been delivered and analyzed in the function of Rician-Shadowed fading severity parameters.

ACKNOWLEDGEMENT

This research has been carried out under the internal-junior project IJ-0204, Faculty of Sciences and Mathematics, University of Priština in Kosovska Mitrovica.

REFERENCES

Abdi, A., Lau, W., Alouini, M., & Kaveh, M. 2003, Cooperative Non-Orthogonal Multiple Access in 5G Systems, IEEE Communication Letters, 19(8), pp. 1462-1465. doi: 10.1109/LCOMM.2015.2441064

Ding, Z., Peng, M., & Poor, H. V. 2015, Cooperative Non-Orthogonal Multiple Access in 5G Systems, IEEE Communication Letters, 19(8), pp. 1462-1465. doi: 10.1109/LCOMM.2015.2441064

Duan, W., Jiang, X., Wen, M., Wang, J., & Zhang, G. 2018, Two-Stage Superposed Transmission for Cooperative NOMA Systems, IEEE Access, 6, pp. 3920-3931. doi: 10.1109/ACCESS.2017.2789193

Gradshteyn, I. & Ryzhik, I. M. 1990, The algorithm for calculating integrals of hypergeometric type functions and its realization in reduce system, In Proceedings of International Symposium on Symbolic and Algebraic Computation, pp. 212-224.

Gradshteyn, I. & Ryzhik, I. M. 2007, Table of Integrals Series and Products (Academic, USA) Hildebrand, E. 1987, Introduction to Numerical Analysis (Dover, USA)

Hildebrand, E. 1987, Introduction to Numerical Analysis (Dover, USA)

Jha, P. & Kumar, D. 2018, Achievable rate analysis of relay assisted cooperative NOMA over Rician fading channels, In Proceedings 4th International Conference on Recent Advances in Information Technology (RAIT), pp. 1-5. doi: 10.1109/RAIT.2018.8388972

Jha, P., Shree, S., & Kumar, D. 2018, An opportunistic-non orthogonal multiple access based cooperative relaying system over Rician fading channels, In Proceedings 4th International Conference on Recent Advances in Information Technology (RAIT), pp. 1-5. doi: 10.1109/RAIT.2018.8388973

Jiao, R., Dai, L., Zhang, J., MacKenzie, R., & Hao, M. 2017, On the performance of NOMA-based cooperative relaying systems over Rician fading channels, IEEE Transaction on Vehicular Technology, 66 (12), 11409–11413

Kim, J. B. & Lee, I. H. 2015, Capacity Analysis of Cooperative Relaying Systems Using Non- Orthogonal Multiple Access, IEEE Communication Letters, 19(11), pp. 1949-1952. doi: 10.1109/LCOMM.2015.2472414

Liang, X., Wu, Y., Ng, D., et al. 2016, Outage probability of nonorthogonal multiple access schemes with partial relay selection, In Proceedings IEEE 27th Annual International Symposium on Personal Indoor and Mobile Radio Communications (PIMRC), pp. 1-6. doi: 10.1109/PIMRC.2016.7794655

Men, J. & Ge. 2016, Non-orthogonal multiple access for multiple antenna relaying networks, IEEE Communication Letters, 19(10), pp. 1686-1689. doi: 10.1109/LCOMM.2015.2472006

Panic, S. & Jayakody, N. 2019, Performance Analysis of NOMA-Based Cooperative Relay Systems over Hoyt Fading Channels, In Proceedings IEEE 89th Vehicular Technology Conference (VTC2019-Spring, pp. 1-5. doi: 10.1109/VTC-Spring.2019.8746517

Panic, S., Stefanovic, M., Anastasov, J., & Spalevic, P. 2013, Fading and Interference Mitigation in Wireless Communications (CRC Press)

Popovic, G., Panic, S., Anastasov, J., Stefanovic, M., & P., S. 2011, Cooperative MRC diversity over Hoyt fading channels, Electrical Review, 87(12), pp. 150-152.

Simon, M. K. & Alouini, M. S. 2005, Digital communication over fading channels (Wiley-IEEE Press).

Wan, D., Wen, M., Ji, F., Yu, H., & F., C. 2018, Non-Orthogonal Multiple Access for Cooperative Communications: Challenges Opportunities and Trends, IEEE Wireless Communications, 25(2), pp. 109-117. doi: 10.1109/MWC.2018.1700134

Wei, Z., Ng, D. K., Yuan, J., & Wang, H.-M. 2017, Optimal resource allocation for power- efficient MC-NOMA with imperfect channel state information, IEEE Transaction on Communication, 65(9), pp. 3944-3961. doi: 10.1109/TCOMM.2017.2709301

CIP - Каталогизација у публикацији
Народна библиотека Србије, Београд

5

BULLETIN of Natural Sciences Research / editor in chief Stefan R. Panić. - [Štampano izd.]. - Vol. 10, no. 2 (2020)- . - Kosovska Mitrovica : Faculty of Sciences and Mathematics, University of Priština, 2020- (Kruševac : Sigraf). - 29 cm

Polugodišnje. - Je nastavak: The University thought. Publication in natural sciences = ISSN 1450-7226. – Drugo izdanje na drugom medijumu: Bulletin of Natural Sciences Research (Online) = ISSN 2738-1013
ISSN 2738-0971 = Bulletin of Natural Sciences Research (Štampano izd.)
COBISS.SR-ID 28586505

Available Online

This journal is available online. Please visit http://www.bulletinnsr.com to search and download published articles.